Spectroscopic Studies of Atmospheric Relevant Air-Aqueous Interfaces

DISSERTATION

Presented in Partial Fulfillment of the Requirements for the Degree Doctor of Philosophy
in the Graduate School of The Ohio State University

By

Maria Roxana Sierra Hernández

Graduate Program in Environmental Science

The Ohio State University

2010

Dissertation Committee:

Heather C. Allen, Advisor

Anne Carey

Harold Walker

Barbara Wyslouzil

Abstract

Atmospheric aerosols have been of great interest for more than a decade because they have been recognized to play a critical role in the uptake and transformation of chemical species in the atmosphere. Aerosols affect the climate of the earth directly by scattering or absorbing light and indirectly by acting as cloud condensation nuclei. The chemical composition of aerosols plays an important role in determining their optical and chemical properties. In particular, aqueous-phase aerosols, being ubiquitous in the atmosphere, are important to understand because of their impact on atmospheric chemistry and climate change.

Marine aerosols are the most abundant biogenic aerosols in the atmosphere. It has been found that the surface of marine aerosols is covered by an organic film. The presence of a surface organic film may affect the chemical, physical, and optical properties of aerosols, which in turn might have effects on different atmospheric processes. The study of the identity and orientation of chemical species at the surface of aerosols at a molecular level is a determining step to understand the interface of aqueous-phase aerosols. The study of atmospheric aerosols is challenging due to their complexity, thus Langmuir monolayers are used in this dissertation as proxies of organic coated aerosols. Since a number of organic compounds are emitted into the atmosphere, mixed Langmuir monolayers of two fatty acids, palmitic acid and stearic acid, with alkyl halides at the air-water interface were investigated. For this, surface pressure-area isotherms were acquired to elucidate the

phase behavior, self-organization, degree of mixing, and stability of the mixed monolayers by analyzing the mean molecular areas (MMA) and surface excess areas. Brewster angle microscopy (BAM) was used to obtain a microscopic picture of the mixed monolayers. Infrared reflection-absorption spectroscopy (IRRAS) and vibrational sum frequency generation (VSFG) spectroscopy were used to examine at a molecular-level the interfacial molecular structure and intermolecular interactions of the monolayers.

It was found that among all the alkyl halide molecules investigated, 1-bromo-pentadecane, $BrC_{15}H_{31}$ (BrPent), 1-bromo-hexadecane, $BrC_{16}H_{33}$ (BrHex), and ClHex, which do not form monolayers by themselves incorporate into the fatty acid monolayers. Analysis of the mean molecular area suggests that at low surface pressures and low x_2 (mole fraction of the alkyl halide) the components of the mixed monolayers are nonideally miscible and that as the surface pressure increases the alkyl halide molecules (BrPent, BrHex and ClHex) are squeezed out. Both IRRAS and VSFG spectra of mixed monolayers showed C-D peaks from the deuterated fatty acids and C-H peaks from the alkyl halide, which confirmed the existence of alkyl halide molecules in the fatty acid monolayer. IRRAS and VSFG spectra confirmed that BrHex molecules are squeezed out of the fatty acid monolayer as the surface pressure increased. Additionally, VSFG spectra revealed that the alkyl chains of both fatty acids (dPA and dSA) keep their all-trans conformation after the incorporation of alkyl halide molecules.

This dissertation also presents the continuation of a different study in which the uptake of gas-phase methyl chloride to the air-water interface was studied. Methyl chloride is of great interest because it is released to the atmosphere in large amounts, which makes it

the principal contributor of organic chlorine to the atmosphere. It was previously shown that CH_3OH is present at the air-water interface and in the bulk aqueous solutions, whereas CH_3Cl was only found in the bulk. Here, the gas phase concentration of CH_3OH and CH_3Cl was measured to determine its possible contribution for the lack of VSFG signal for CH_3Cl. Our findings revealed that the number of CH_3Cl molecules in the gas phase was larger than the number of gas phase CH_3OH molecules and therefore it is not a factor for the lack of VSFG signal. The length of the experiment was tested to determine if it was a factor for the lack of VSFG signal for CH_3Cl. The results showed that the systems were at equilibrium. Therefore, the length of the CH_3Cl experiment was not a limiting factor for the lack of SFG signal of CH_3Cl. The results previously published and those of this chapter suggest that orientation (disordered molecules) and low number density explain the absence of the CH_3Cl signal in the SFG spectrum.

Additionally, the air-aqueous interface of aqueous HBr and NaBr solutions was investigated using VSFG. Enhanced intensity was observed in the water OH stretching modes of the HBr solutions. The SFG spectra reveal a surface proton continuum at frequencies below 3000 cm^{-1}, indicating that hydronium ions and Zundel ions (H_3O^+ and H_5O^{2+}) exist at the air-water interface.

Acknowledgments

There are many people I would like to thank who helped me in different ways in achieving this goal. First of all, I wish to thank my advisor, Dr. Heather Allen for providing the guidance and support necessary to accomplish this degree. I would also like to thank past and present member of the Allen group. In particular Dr. Gang Ma who was always available to answer any kind of questions; Dr. Lisa Van Loon for her scientific and general help during my first years at OSU. I also wish to thank to Dr. Nadia Casillas for all the invaluable helped with the SFG experiments and the SFG discussions. I would also like to thank Hardy Castada for her assistance with all the BAM experiments in Chapter 3.

I wish to thank my family for their constant encouragement and support. I would also like to thank Dr. Lina Yousef for her friendship and for providing the fun needed to complete this journey. Finally, I want to thank my good friends Elisa and Fareeda, for all those concerts which were necessary to keep my sanity through this process.

Vita

Publications

- Allen, H. C., Casillas-Ituarte, N. N. Sierra-Hernández, M. R. Chen, X. and Tang, C. Y. Shedding light on water structure at air–aqueous interfaces: ions, lipids, and hydration. Physical Chemistry Chemical Physics, 2009, 11, 5538-5549.

- Harper, K., Minofar, B. Sierra-Hernández, M. R., Casillas-Ituarte, N. N., Roeselová, M. and Allen. H. C. Surface residence and uptake of methyl chloride

and methyl alcohol at the air/water interface studied by vibrational sum frequency spectroscopy and molecular dynamics. Journal of Physical Chemistry A, 2009, 113, 2015-2024.

- Levering, L. M., Sierra-Hernández, M. R. and Allen. H. C. Observation of hydronium anions at the air-aqueous acid interface: Vibrational spectroscopic studies of aqueous HCl, HBr, and HI, for special issue in Honor of Kenneth B. Eisenthal. Journal of Physical Chemistry C, 2007, 111, 8814-8826

Fields of Study

Major Field: Environmental Science.

Table of Contents

List of Tables

List of Figures

List of Abbreviations

a.u.	arbitrary units
BAM	Brewster angle microscopy
BrHex	1-bromo hexadecane
BrPent	1-bromo pentadecane
°C	degrees Celsius
CCD	charge-coupled device
ClHex	1-chloro hexadecane
cm^{-1}	wavenumbers
dPA	deuterated palmitic acid
dSA	deuterated stearic acid
FTIR	Fourier transform infrared
G	gas phase
Hz	hertz
IR	infrared
IRRAS	infrared reflection absorption spectroscopy
LC	liquid condensed phase
MCT	mercury cadmium telluride detector
MMA	mean molecular area
μl	microliter
μJ	microJoule
mM	millimolar
mW	milliwatt
PMT	photomultiplier

R	reflection
RA	reflection-absorbance
RX	alkyl halide
SFG	sum frequency generation
TC	tilted condensed phase
UC	untilted condensed phase
Vis	visible
x	mole fraction

Chapter 1

Introduction

This dissertation presents studies of atmospheric relevant air-aqueous interfaces. These include mixed monolayers of fatty acids with alkyl halides, the uptake of gas-phase alkyl halides and alcohols, and the presence of hydrogen halide at the air-water interface. These studies were performed to understand better the surface structure of atmospheric aerosols.

Aerosols are defined as solid or liquid particles suspended in the air. They come from a variety of sources such as biomass burning, volcanic eruptions, fossil fuel burning, windblown soils, and the wave action from the ocean.

Aerosols are ubiquitous in the atmosphere and play important roles in the troposphere affecting human health, the air quality, and the climate.[1,2] They have been associated with asthma,[3] lung cancer, and cardiovascular diseases.[4] They affect the climate of earth directly by scattering light leading to cooling or by absorbing and emitting light contributing to the warming of the troposphere. Aerosols can also affect the climate indirectly by acting as cloud condensation nuclei (CCN) which can result in the reduction of precipitation.[1,5,6] Additionally, aerosols play a crucial role in the stratosphere acting as nuclei for polar stratospheric cloud formation. Furthermore, aerosols provide the surface

for heterogeneous reactions in the stratosphere. The ozone hole in the stratosphere is the result of heterogeneous reactions on polar stratospheric clouds in which chlorine and bromine atoms are released. [7] The effect of aerosols on climate has a large uncertainty as shown in the assessment reports by the Intergovernmental Panel on Climate Change (IPCC).[5]

The chemical composition of an aerosol plays an important role in determining its optical and chemical properties.[8] Atmospheric aerosols are usually composed of a mixture of organic and inorganic compounds. In many cases, the composition of particles varies considerably within one air mass. Thus, measurement aerosol chemical composition is difficult, but important advances in this field have been achieved through the use of aerosol mass spectrometry.[9-12]

Atmospheric aerosol surface chemistry also plays a critical role in the uptake and transformation of gaseous species in the atmosphere.[8,13] Single-phase reactions are very important in atmospheric chemistry reactions. However, in the last two decades it has been demonstrated that heterogeneous reactions on the surface of aerosols have to be taken into account for all atmospheric processes. Among many examples, Molina et al[7] showed that the reaction between HCl and $ClONO_2$ proceeds faster on an ice surface than in gas phase. Similarly, Hu et al[14] studied the uptake of gas-phase Cl_2 and Br_2 by aqueous surfaces containing Br^- and I^-. They found that reactions at the air-aqueous interface play a critical role in determining the gas uptake. Also, Jayne et al[15] reported that the oxidation of SO_2 to sulfate is facilitated by the formation of a complex at the air-aqueous interface between SO_2 and H_2O. Later, Donaldson et al[16] observed the complex with second

harmonic generation spectroscopy. Therefore, it is fundamental to investigate the identity and orientation of the species at the surface of aerosols that can affect the physical characteristics of their surface and thus influence the initial adsorption of gas-phase molecules.

The focus of the studies presented in this dissertation is on the fundamental physical chemistry of atmospheric relevant interfaces. An understanding of the molecular organization at relevant aqueous surfaces is a necessary step. The finding of fundamental studies can be extrapolated to atmospheric conditions.

Marine aerosols are formed by the wave action from the surface ocean. The IPCC has estimated that 3.3 billion metric tons of salt spray enters the atmosphere yearly. Previously, Duce and coworkers[17] found that fatty acids are enriched in the surface ocean and they suggested that the surface of marine aerosols can also be enriched by pollutants. Zafiriou et al detected fatty acids in marine aerosols in the tropical North Pacific.[18] Gill et al.[19] proposed in 1983 the existence of marine aerosols coated with hydrophobic organic monolayers. Fat-coated aerosols were described as inverse micelles with the polar head of the carboxylic groups of the fatty acids (R-COOH) oriented into the water droplet and the alkyl chains oriented out toward the atmosphere. Tervahattu et al.[20,21] found that fat-coated aerosols exist in both marine and continental aerosols. They found that fatty acids such as palmitic acid (PA) and stearic acid (SA) as well as other acids of different alkyl-chain length up to the C_{32} acid covered marine aerosols. Such organic films may affect the chemical, physical, and optical properties of aerosol particles, which in turn might have effects on different atmospheric processes. A great number of organic compounds

3

are emitted into the atmosphere from both biogenic and anthropogenic sources, therefore it should be expected that a variety of organics exist within the surface region of atmospheric aerosols. Langmuir monolayers are used as proxies for organic coated aerosols. Chapter 3 presents the investigation of mixed Langmuir monolayers of PA and SA with different alkyl halides at the air-water interface as a fundamental study to understand the surface of fat-coated aerosols and alkyl halides.

Halogenated organic compounds are emitted to the atmosphere by both biogenic and anthropogenic sources. Methyl chloride (CH_3Cl) is the main contributor of reactive chlorine in the atmosphere. Previously,[22] the surface residence and organization of gas-phase methyl chloride (CH_3Cl), butyl chloride (C_4H_9Cl), and butyl bromide (C_4H_9Br) and their corresponding alcohol molecules adsorbed to the air-water interface were investigated. A continuation of that investigation is presented in Chapter 4 of this dissertation. In Chapter 5, the air-water interface is investigated in the presence of HBr and NaBr. Finally, the atmospheric implications of these results are discussed in Chapter 6.

Chapter 2

Instrumentation

An overview of the theory of infrared reflection absorption spectroscopy (IRRAS), vibrational sum frequency generation spectroscopy (VSFG), and Brewster angle microscopy (BAM) is presented in this chapter. Instrumental and experimental details are also presented. Experimental details relevant to each experiment are provided in particular chapters.

2.1 Theories

Infrared Reflection Absorption Spectroscopy (IRRAS)

IRRAS is a spectroscopic technique to study the chemical composition and orientation of molecules at an interface. An infrared (IR) beam is directed onto an interface at an incident angle and the reflected beam provides a vibrational spectrum. A schematic drawing of the experimental set-up used in here is shown in Figure 2.1.

IRRAS spectra are presented as reflection-absorbance (RA) spectra:

$$RA = -\log \frac{R}{R_0} \tag{2.1}$$

where R is the IR reflectivity of the monolayer-covered surface, and R_0 is the IR reflectivity of the bare water subphase.

RA spectra depend on the molecular properties of the monolayer molecules and also on the optical effects due to the reflection properties of the interface.

When light travels in a medium different than vacuum, it experiences two effects, a speed reduction described by the real refractive index, n; and attenuation described by an extinction coefficient, k. The complex refractive index ($\tilde{n}$) comprises these two quantities:

$$\tilde{n} = n + ik \tag{2.2}$$

R is a function of the wavenumber (ν) and depends on the angle of incidence of the IR beam with respect to the normal surface(θ), the optical properties of the material ($\tilde{n}$), and the polarization of the IR beam.[23-25] It is measured as the reflected light intensity (I_R) with respect to the incident intensity (I_0) as shown in eq 2.3

$$R = \frac{I_R}{I_0} \tag{2.3}$$

Reflectivity values are calculated by multiplying the respective complex reflection coefficient ($\tilde{r}$) with its complex conjugate ($\tilde{r}^*$), eq 2.4

$$R = \tilde{r}\tilde{r}^* \tag{2.4}$$

The reflection coefficients can be calculated from the Fresnel equations for s and p polarization. The s and p polarizations are light polarized with its electric vector oscillating perpendicular and parallel to the plane of incidence. The electric vector in p polarization has components in the x and z axes, whereas that in s polarization has only components in the y axis (Figure 2.2).

6

The reflection coefficients used to describe the IRRAS bands in a three phase system monolayer at an interface (Figure 2.2), were developed by Kuzmin and Michailov[23,26]

$$\tilde{r}_s = -\frac{\sin(\theta_0 - \tilde{\theta}_2) - ik_o\tilde{n}_2^{-1}\sin\theta_1\tilde{I}_1}{\sin(\theta_0 + \tilde{\theta}_2) - ik_o\tilde{n}_2^{-1}\sin\theta_1\tilde{I}_1} \tag{2.5}$$

$$\tilde{r}_p = \frac{\sin(\theta_0 - \tilde{\theta}_2)\cos(\theta_0 + \tilde{\theta}_2) - ik_o\tilde{n}_2^{-1}\sin\theta_1(\tilde{I}_1\cos\theta_1\cos\theta_2 - \tilde{I}_2\sin\theta_1\sin\theta_2)}{\sin(\theta_0 + \tilde{\theta}_2)\cos(\theta_0 - \tilde{\theta}_2) - ik_o\tilde{n}_2^{-1}\sin\theta_1(\tilde{I}_1\cos\theta_1\cos\theta_2 + \tilde{I}_2\sin\theta_1\sin\theta_2)} \tag{2.6}$$

In which

$$\tilde{I}_1 = \int(\tilde{n}_x^2(z) - n_2^2)dz \tag{2.7}$$

$$\tilde{I}_2 = \int\frac{(\tilde{n}_z^2(z) - n_2^2)dz}{\tilde{n}_z^2(z)}dz \tag{2.8}$$

$\tilde{n}_x$ and $\tilde{n}_z$ are the complex directional refractive indices of the monolayer.

The reflectivity (R) of the film can be calculated with eq 2.4 and the reflectance-absorbance (RA) with eq 2.1.

As mentioned above, R of an interface as described by the Fresnel equations of reflection is a function of the refractive index of the medium, the angle of the incident IR beam and its polarization, and the wavenumber. A detailed description of the Fresnel equations and the RA for different angles of incidence and polarizations can be found somewhere else.[23,27] For dipoles oriented perpendicular to the chain axis such as the methylene vibrations, R increases with the angle of incidence with s polarization. RAs bands intensities decrease with increasing the angle of incidence and are negative at all the incident angles. Hence, using s polarized light, IRRAS spectra show negative peaks. On the other hand, Rp decreases to zero at the Brewster angle to increase again passing

7

the Brewster angle and therefore, IRRAS spectra obtained with p polarized light show negative or positive peaks, depending on the angle of incidence. RAp bands intensities show two maximums close to the Brewster angle.[23]

Vibrational Sum Frequency Generation (VSFG)

VSFG is a second-order nonlinear spectroscopic technique that provides vibrational spectra of molecules at interfaces. Detailed descriptions of the VSFG theory can be found in the literature. [28-30] A brief descriptions is given here.

VSFG is the generation of a sum frequency beam by two laser beams of different frequencies, one of fixed visible frequency (ω_{VIS}) and the other of tunable infrared frequency (ω_{IR}), overlapped at the surface sample in space and time. The frequency of the resulting SFG beam is the sum of the frequencies of the two incident beams. When the infrared frequency is resonant with a vibrational mode of an interfacial molecule, the SFG signal is enhanced.

VSFG intensity arises only from environments that lack inversion of symmetry such as interfaces. This rule makes VSFG unique as a surface selective technique. The intensity of the SFG signal (I_{SFG}) is proportional to the intensities of the incident beams (infrared, I_{IR} and visible, I_{VIS}) as shown in eq 2.9

$$I_{SFG} \propto \left| \chi^{(2)} \right|^2 \cdot I_{IR} I_{VIS} \tag{2.9}$$

where $\chi^{(2)}$ is the macroscopic second-order nonlinear susceptibility. $\chi^{(2)}$ is comprised of a nonresonant term ($\chi_{NR}^{(2)}$) and the sum of resonant terms ($\chi_{v}^{(2)}$), eq 2.10

$$\left|\chi^{(2)}\right|^2 = \left|\chi_{NR}^{(2)} + \sum_v \chi_v^{(2)}\right|^2 \tag{2.10}$$

When the frequency of the incident infrared beam is resonant with a vibrational mode of the molecules adsorbed at the interface, the resonant term dominates the nonlinear susceptibility $\chi^{(2)}$ and an enhancement of SFG signal is observed. $\chi_v^{(2)}$ is proportional to the number density of the surface species (N) and to the molecular hyperpolarizability for the vibrational mode v (β_v) of that vibration through the Euler angle transformation ($\mu_{IJK \cdot lmn}$) between the laboratory coordinates (I, J, K) and the molecular coordinates (l, m, n), eq 2.11

$$\chi_v^{(2)} = N \sum_{lmn} \langle \mu_{IJK \cdot lmn} \rangle \beta_v^{lmn} \tag{2.11}$$

where $\langle\ \rangle$ represents an average over the orientational distribution of the molecules. The molecular hyperpolarizability is proportional to the Raman polarizability tensor (α) and to the infrared transition moment (μ) as shown in eq 2.12

$$\beta_v^{lmn} = \frac{-\mu_{v0}^n (\alpha_{v0}^{lm})}{2\hbar(\omega_{IR} - \omega_v + i\Gamma_v)} \tag{2.12}$$

where ω_{IR} is the frequency of the incident IR beam, ω_v is the resonant frequency, and Γ_v describes the half-width at half maximum of the transition. When the frequency of the incident IR beam approaches the frequency of the vibrational mode, $\omega_{IR} - \omega_v$ approaches

9

zero and $\chi_\nu^{(2)}$ increases, which results in an increase of the SFG signal. β_ν^{lmn} is nonzero only when both Raman and the IR transition moments are nonzero which shows that for a vibrational mode to be SFG active, it must be Raman and IR active. Symmetry constraints arising from this selection rule lead to the requirement for a lack of inversion symmetry for sum frequency generation to be allowed. Macroscopically, this requirement is fulfilled at interfaces between two isotropic bulk phases.

Brewster Angle Microscopy (BAM)

The principle of BAM has been described in detail elsewhere.[31,32] Briefly, air-water interfaces form a boundary between two different media that differ in refractive index. When an air-water interface is irradiated with p-polarized light at the Brewster angle (eq 2.13), no light is reflected from such interface (Figure 2.3a) and black background will be observed in the BAM image.

$$\tan[\theta_B] = \frac{n_2}{n_0} \tag{2.13}$$

Eq 2.13 shows that the Brewster angle (θ_B) is determined by the refractive index of air (n_0) and water (η_2) for an air-water interface. For pure water, the Brewster angle is 53°. The addition of a Langmuir monolayer modifies the refractive index of the interface. As a result, the monolayer reflects p-polarized light and forms an image that can be seen by BAM (Figure 2.3b). The BAM image results from a change in the refractive index of the system and an increase in molecular density at the air-water interface. As the monolayer becomes denser, brighter images appear. Thus, bright regions of an image represent an

area of high intermolecular organization in the monolayer and are typically referred as "domains". Dark regions represent a less ordered, more expanded region of the monolayer.

2.2 Instrumentation

IRRAS

IRRAS spectra were obtained using a PerkinElmer Spectrum 100 FTIR Spectrometer equipped with a nitrogen-cooled MCT (mercury cadmium telluride) detector. Two 2-in. diameter gold mirrors were positioned apart on a breadboard in the FTIR chamber to direct the IR beam to and from the air-water interface with a 40° angle of incidence with respect to the surface normal. The Brewster angle for this interface is 53°. The Langmuir film balance was placed on the breadboard in the FTIR chamber (Figure 2.4).

SFG

Two different SFG systems were used in the studies presented in this dissertation, a broad bandwidth SFG (BBSFG) and a scanning 20 Hz SFG.

Details of the BBSFG have been described elsewhere.[33,34] The BBSFG is a Ti:sapphire-based ultrafast system (Spectra Physics) that utilizes two amplifiers to produce 2 picosecond and 100 femtosecond pulses. The picosecond pulses are used to produce a narrow bandwidth of 800 nm, whereas the femtosecond pulses are used to pump an optical parametric amplifier (OPA) to produce a broad bandwidth (~200 cm^{-1}) of infrared pulses. The generated SFG signal containing spectral information from the

monolayer was detected using a monochromator-CCD detection system (Acton Research, SpectraProSP-500 monochromator with a 1200 g/mm grating blazed at 750 nm; Roper Scientific, 1340 x 400 pixel array, LN400EB back illuminated CCD). The SFG spectrum is polarization dependent, where the polarization combinations used were ssp and ppp for the SFG, 800 nm, and infrared beams, respectively.

SFG spectra for the studies presented in Chapter 5 were acquired using the 20 Hz scanning VSFG system from EKSPLA. In this system, a 1064 nm EKSPLA PL 2143A/20/SS Nd:YAG laser (27 ps pulse duration and 20 Hz repetition rate) pumps an EKSPLA PG401/DFG2-16P optical parametric generator (OPG). The peak IR energy at 2940 cm^{-1} was 51 µJ per pulse whereas the visible energy at 532 nm was 370 µJ per pulse. The input angles for the 20 Hz visible and infrared beams were 66.3° and 56.8°, respectively. A photomultiplier tube (PMT Hamamatsu, R5929) was used to detect the SFG signal.

BAM

The generalized Brewster angle microscope setup is shown in Figure 2.5. A REO HeNe laser beam incident of a 633 nm, 17 mW strikes the air-water interface at the Brewster angle. A neutral density filter after the laser is placed to reduce the amount of light that will pass through a glan laser polarizer which allows only p-polarized light to strike the air-water interface. A black glass plate is placed at the bottom of the Langmuir trough to absorb any incident light that penetrates the aqueous subphase. Any light reflected by the surface passes through a 20x objective lens. After passing through the objective lens, the

12

reflected light is focused by a focusing lens into a 512 x 512 pixel-CCD camera (Andor, model DV 412) is used to acquire BAM images in real time. The CCD sends BAM images to the computer through a USB connection. A.
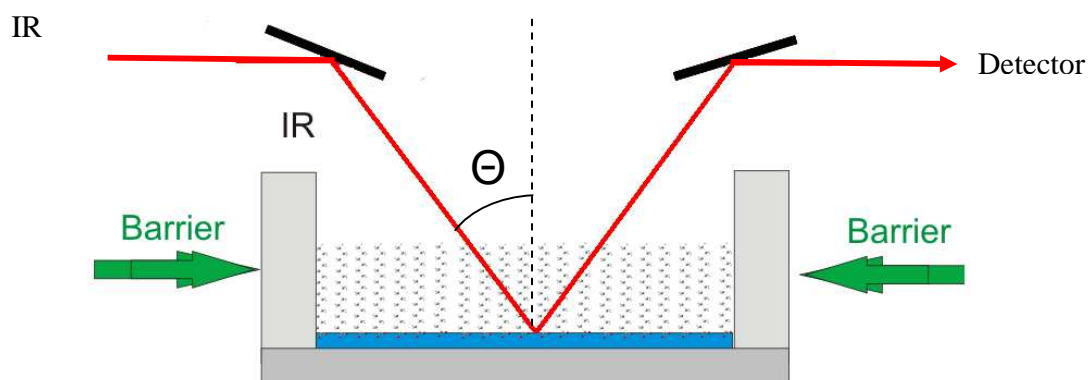
Figure 2.1 Schematic drawing of a set-up for IRRAS to analyze the chemical composition of a monolayer at the air-water interface. It consists of a Langmuir trough filled with nanopure water and a monolayer of the molecules of interest spread on it. An IR beam is directed onto the air-water interface at an incident angle (Θ) and the reflected beam is directed to a detector to obtain a vibrational spectrum.

air

θ_0

$n_0=1$

monolayer

θ_1

$\tilde{n}_x = n_x - ik_x$

$\tilde{n}_y = n_y - ik_y$

$\tilde{n}_z = n_z - ik_z$

water

θ_2

$\tilde{n}_2 = n_2 - ik_2$

Z

Y

X
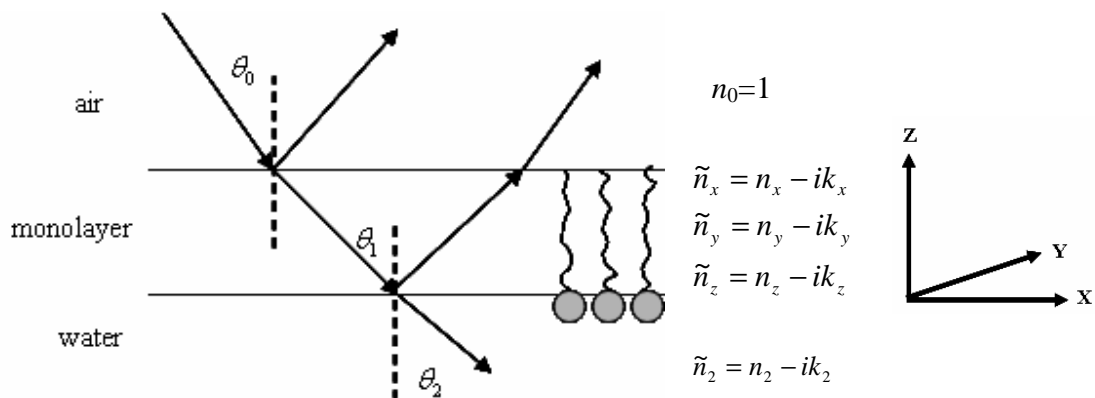
Figure 2.2 Schematic view of a three phase system (monolayer at an air-water interface) used to determine reflection coefficients and the axis system used for describing IRRAS geometry. n_x, n_y, and n_z are the directional refractive indices of the monolayer.
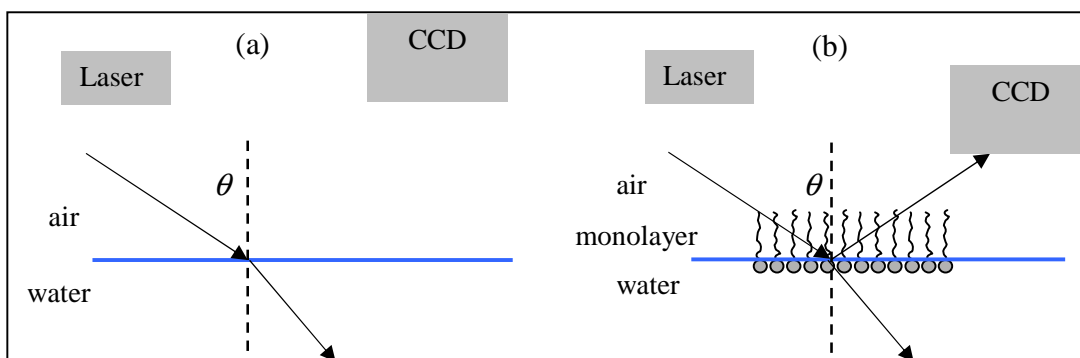
Figure 2.3 Scheme of the BAM principle. When an incident p-polarized light source shines on an air-water interface at the Brewster angle (θ), no light is reflected (a). The addition of a Langmuir monolayer modifies the refractive index of the interface and p-polarized light is reflected forming an image that can be seen by BAM (b).
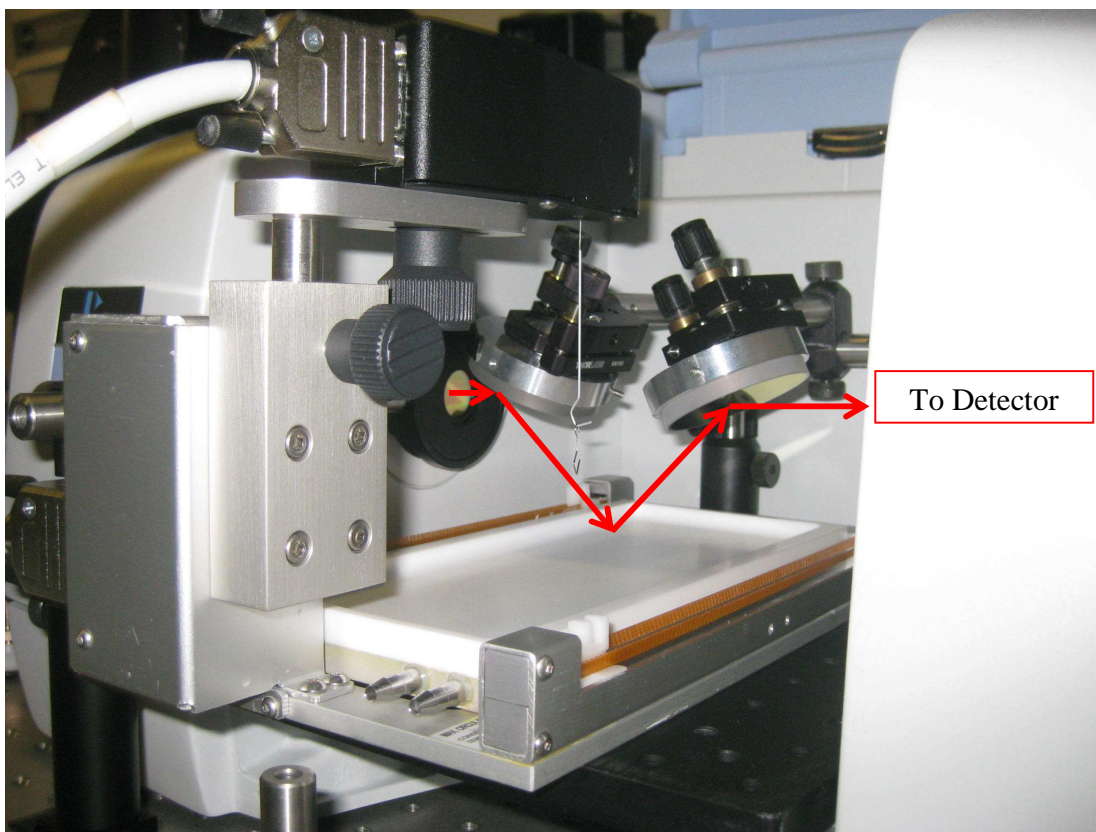
Figure 2.4 IRRAS set-up used in the Allen lab. It consists of a ZnSe wire grid polarizer before the gold mirror that directs the IR beam to the air-water surface. A second gold mirror directs the reflected IR beam to the MCT detector.
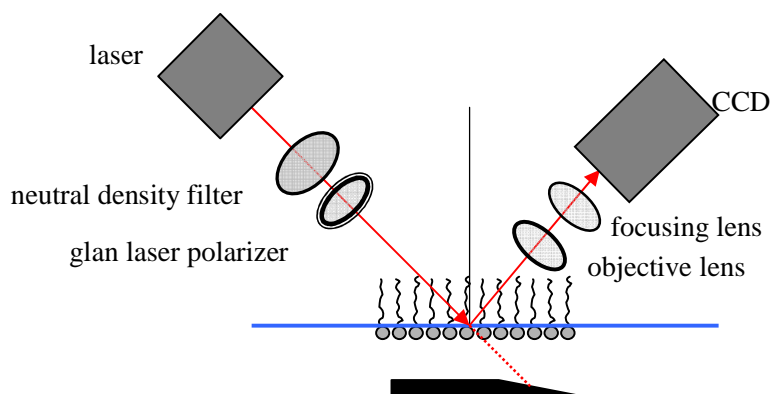
Figure 2.5 BAM instrument in the Allen lab. It consists of a REO HeNe laser beam incident of 633 nm, a neutral density filter and a glan laser polarizer which allows only p-polarized light to strike the air-water interface. A black glass plate is placed at the bottom of the Langmuir trough to absorb any incident light that penetrates the aqueous subphase. Light reflected by the surface passes through a 20x objective lens and a focusing lense before reaching a 512 x 512 pixel-CCD camera.

Chapter 3

Mixed Monolayers of Long Chain Alkyl Halides and Fatty Acids at the Air-Water Interface

Langmuir monolayers are normally formed by amphiphilic molecules with a hydrophilic head group and a hydrophobic chain. The stability of a monolayer depends on the chemical and physical properties of the film. Fatty acids such as PA form stable monolayers at the air-water interface by themselves. Long chain alkyl halides do not form monolayers by themselves; however, they can be incorporated into existing monolayers.[35-37]

A complex array of organics is emitted into the atmosphere, thus the surfaces of aerosols are expected to have a highly complex composition.[8] Mixed monolayers are therefore appropriate models to understand aerosol surfaces. Mixed Langmuir monolayers are monomolecular films containing more than one chemical species.[38] In this investigation, mixed monolayers of two fatty acids, deuterated palmitic acid, $C_{15}D_{31}COOH$ (dPA) and deuterated stearic acid, $C_{17}D_{35}COOH$ (dSA) with alkyl halides (1-bromo-alkanes) of different carbon-chain length and 1-chloro-hexadecane at the air-water interface were investigated. Previously we have investigated fatty acid films,[39-41] as have many others.[31,38,42-47] Palmitic acid and stearic acid were chosen for this

investigation because they have been found in abundance in the organic surface layer of marine aerosols.[20,21] Halogenated organic compounds from both biogenic and anthropogenic sources are emitted into the atmosphere. Of the alkyl halides, short-chain alkyl halides have been found in the atmosphere, in addition to the oxidization products of halogens.[48] Of the alkyl halides, methyl chloride (CH_3Cl),[49,50] methyl bromide (CH_3Br),[8] methyl iodide (CH_3I)[51], ethyl iodide (C_2H_5I), and 1-propyl iodide (C_3H_7I)[52] as well as CH_3CCl_3, CH_2Cl_2, and variations of $CH_xCl_yBr_z$ among others[8,53] have been identified and discussed. Although longer chain alkyl halides have not been identified in the atmosphere, many marine organisms contain significant quantities of brominated organic compounds (BOCs; $\gg C_2$), some of which have anthropogenic origins from bioaccumulation of brominated flame retardants.[54-56] We therefore assert that atmospheric aerosol surface films will also be comprised of these BOCs.

The first step for this investigation was to determine the minimum chain-length of alkyl halide that incorporates into dPA and dSA monolayers by conducting surface pressure-area isotherms. For this, alkyl bromide molecules from C_3 to C_{16}-chain length were tested. Only C_{15} and C_{16} alkyl bromides spread with dPA and dSA as films revealed a surface pressure change relative to the pure dPA and dSA surfaces. Here we present the thermodynamic and spectroscopic results of dPA and dSA mixed with those alkyl halides that incorporated into the fatty acid monolayer.

This chapter is organized as follows. Surface pressure-area isotherms are shown to understand the phase behavior and self-organization of mixed monolayers. Vibrational sum frequency generation (SFG) spectroscopy data are presented to understand how the

alkyl halide molecules affect the conformations of the fatty acid molecules. Then, IRRAS spectra of two different systems dSA-BrHex (3:1 and 1:1) and dPA-BrHex (3:1 and 1:1) are presented to elucidate further the chain ordering and to track surface number densities. In addition, Brewster angle microscopy (BAM) images are shown to provide an alternate view of the morphological film parameters such as film homogeneity, domain size, shape and packing, and to shed further light on miscibility.

Commonly used acronyms: dPA, deuterated palmitic acid; **dSA**, deuterated stearic acid; **BrPent**, 1-bromo pentadecane; **BrHex**, 1-bromo hexadecane; **ClHex**, 1-chloro hexadecane; **BAM**, Brewster angle microscopy; **MMA**, mean molecular area; **G**, gas phase; **LC**, liquid condensed phase; **LE**, liquid expanded phase; **TC**, tilted condensed phase; **UC**, untilted condensed phase; **R**, reflectance; **RA**, reflectance-absorbance; **RX**, alkyl halide; **SFG**, sum frequency generation.

3.1 Experimental

3.1.1 Materials

Deuterated palmitic acid, $C_{15}D_{31}COOH$ (dPA) and deuterated stearic acid, $C_{17}D_{35}COOH$ (dSA) with 98% purity were obtained from Cambridge Isotope Laboratories, Inc. Alkyl halides (RX) were used as received from Acros Organics without further purification. Solutions of each were prepared in chloroform (>99.8%, HPLC grade, Fisher Scientific). Monolayers were spread on deionized water with a resistivity of 18.2 MΩ·cm (Barnstead Nanopure filtration system). All experiments were conducted at room temperature (22°C ± 1°C) and at atmospheric pressure.

3.1.2 Methods

Langmuir Film Balance. Surface pressure-area isotherms were performed with a KSV minitrough (KSV Instruments, Finland). The trough is made of Teflon and has dimensions of 176.5 x 85 mm. The film compression was symmetrically performed by two inter-linked surface barriers. The barriers are made of Delrin, which prevents leakage of the monolayer under the barriers. The surface pressure and mean molecular area (MMA) were continuously monitored during film compression by the Wilhelmy plate method. Filter paper plates were used (Whatman ashless filter paper #41). The trough was filled with pure water (Nanopure) as the subphase. The aqueous subphase was replaced after each experiment. Before spreading the sample on the subphase, the subphase was swept by the barriers to ensure that there was no significant surface pressure increase upon compression. Stock solutions of dPA, dSA, and of each alkyl halide were prepared in chloroform with a concentration of 2 mM. Mixed solutions of dPA/RX, and dSA/RX were prepared by mixing desired amounts of the stock solutions. Three different mole ratios of dPA or dSA to each RX were used, 3:1, 1:1, and 1:3. A measured volume of lipid solution or mixture was spread on the subphase surface in a dropwise manner with a Hamilton syringe and 15 minutes elapsed for complete chloroform evaporation. The barriers were compressed at a speed of 5mm/min.

Vibrational Sum Frequency Generation (Broad Bandwidth Technology). The Langmuir film balance was placed on the sample stage of the SFG system. The IR and visible beams are overlapped at the monolayer surface spatially and temporally. SFG spectra

were obtained with a 5-min acquisition time as a function of incident infrared wavelength of dPA-BrHex 1:1 and dPA monolayers at the air-water interface at 5, 18, and 25 mN/m. SFG spectra were taken under the hold mode of the film balance. In this mode, the barriers move to compensate for the surface pressure drop and a constant pressure is therefore retained. Background spectra were obtained for each sample by disrupting the temporal overlap of the beams. The background spectra are subtracted from the sample spectra and the resulting spectra are normalized to the nonresonant signal from a GaAs crystal surface (Lambda Precision Optics, Inc) to remove the spectral distortion caused by the energy profile of the infrared pulse.

To calibrate the SFG peak positions in the C-H stretching region, a nonresonant SFG spectrum from the GaAs crystal surface was obtained with a polystyrene film covering the infrared output port of the optical parametric amplifier. The resulting SFG spectrum containing polystyrene infrared absorption bands was used for the calibration. To calibrate the SFG peak positions in the C-D stretching region, the absorption bands of ambient CO_2 vapor were used.

IRRAS. Spectra were acquired using the IRRAS as described in Chapter 2, section 2.2. Spectra were collected at a resolution of 4 cm^{-1} and averaged over 300 scans. All spectra were collected with s and p polarized light by positioning a ZnSe wire grid polarizer (Janos Technology Inc.) before the gold mirror that directed the IR beam to the air-water surface.

BAM Imaging. A home-built BAM was used for imaging the monolayer film morphology from monolayers formed utilizing the same KSV minitrough used in the isotherm studies (Chapter 2, Section 2.2) The BAM light source (HeNe at 632.8 nm and 17 mW) is positioned at 53°, which is the Brewster angle for neat water. Monolayers were compressed at a rate of 5 mm2/min. An acquisition time of 0.018 s and a delay of 8.923 s for the CCD to process the image were used.

3.2 Results and Discussion

3.2.1 Surface Pressure-Area Isotherms

Surface pressure-area isotherms were obtained after spreading the pure compound solutions on a pure water subphase. Figure 3.1a shows the isotherms of pure dPA, dSA, BrPent, BrHex, and ClHex films. Surface pressure-area isotherm measurements describe the phase behavior of Langmuir monolayers.[38] BrPent, BrHex, and ClHex isotherms show a constant surface pressure of zero indicating that the alkyl halides do not form monolayers at the air-water interface as expected.[38] dPa and dSA isotherms exhibit surface pressure states that are in good agreement with PA and SA isotherms reported previously.[38,57] The shape of the isotherms and regions of constant slope correspond to different phases. The observed phases have previously been assigned as gas-tilted condensed (G-TC), tilted condensed (TC), untilted condensed (UC), and collapsed phases.[39,40,46] At 0 mN/m, the G phase is in coexistence with the TC phase as evidenced from our BAM images and is discussed below in Section 3.2.4.

In Figure 3.1a, interpreting the isotherms from right to left, the surface pressure of the dPA and dSA monolayers start to increase at 26 Å/molecule and 24 Å/molecule, respectively, indicating that the surface organization of the dPA and the dSA monolayers changes from a G-TC coexistence phase to a TC phase. The isotherms show a kink at 25 mN/m for dPA and 27 mN/m for dSA, indicating a second order phase transition from the TC phase to the UC phase.[46] Film collapse occurs at 40 mN/m for dPA, and at 50 mN/m for dSA. Also observed, the dSA isotherm lies to the left of the dPA isotherm. Nutting and Harkins[57] showed that the molecular area of the condensed phase decreases with the length of the hydrocarbon chain resulting from the van der Waals energy increases with the length of the hydrocarbon chain.

As mentioned in the Introduction, the first step of this investigation was to determine the minimum alkyl chain-length of alkyl halides to be incorporated into a fatty acid monolayer at the air-water interface as observed by a change in the isotherm relative to that of the pure fatty acid. Incorporation of the shorter-chain 1-bromo alkanes, C_4 to C_{10}, was not observed. From the longer-chain 1-bromo-alkanes, BrPent and BrHex in 1:1 mixtures were observed to incorporate as shown in Table 3.1. A minimum of 15 carbons is needed to incorporate. However, this result does not mean that such bromo-alkanes will form miscible mixed monolayers. Discussion of the isotherms is presented below with an extended thermodynamic analysis to further evaluate their miscibility is provided in the Appendix A.

In addition to the bromo-alkanes, incorporation studies of C_{15} and C_{16} alkanes were completed. It was observed that pentadecane and hexadecane, contrary to the

corresponding bromo-alkanes, do not incorporate into fatty acid monolayers as shown by an unchanged isotherm relative to that of the pure fatty acid. The halogen head group of a bromo-alkane is not as polar compared to the COOH of a fatty acid (dPA and dSA). However, the C-Br bond of a bromo-alkane is slightly more polar than the C-H bond of an alkane.[22] Thus, a C-Br bond is more likely to associate with water molecules than a terminal C-H bond of an alkane. These intermolecular forces only partially explain the observed incorporation into the monolayer since chain length is apparently more important than the dipole-dipole interactions of C-Br with surface water molecules.

C_{15}, C_{16} Alkyl Halides, and dPA Mixed Monolayers. Figure 3.1b shows the surface pressure-area isotherms of dPA-BrPent, dPA-BrHex, and dPA-ClHex mixed monolayers with a mole ratio of 1:1. If there were no incorporation of the alkyl halide, one would expect to see the isotherm of the mixed monolayer overlapped onto the pure fatty acid isotherm. The first obvious feature in Figure 3.1b is the shift of the pure dPA isotherm to larger areas upon addition of BrPent, BrHex and ClHex, which suggests incorporation of the respective alkyl halide into the dPA monolayer. This is more evident at low surface pressures, whereas at high surface pressures the isotherms become slightly closer to the pure dPA isotherm in most cases. The increase in MMA represents the area occupied by the alkyl halides.

The dPA-BrPent isotherm (Figure 3.1b-2) shows a phase that does not exist in that of the pure dPA isotherm. As the dPA-BrPent mixed monolayer is compressed, there seems to be a transition from a G to a liquid expanded (LE) phase at 57 Å^2/molecule. The dPA-

BrPent isotherm lifts at 57 Å^2/molecule with a very small slope. This region corresponds to the LE phase. In the LE phase, the hydrophobic chains of the molecules are thought to be randomly oriented with many gauche defects, whereas in the G phase, in addition to having the hydrophobic chains randomly oriented, the molecules are on average far apart from each other. Kaganer et al[46] defined the LE phase as the region in which molecules behave like a two-dimensional (2D) liquid where the headgroups of the molecules are translationally disordered and the chains are conformationally disordered. For all phases the polar head groups are submerged in the aqueous subphase.[38] As the monolayer is compressed further to 34 Å^2/molecule and a surface pressure of 3 mN/m, the TC transition occurs. The slope of the curve in the TC phase is slightly smaller than that of the pure dPA. This suggests that some BrPent molecules are being squeezed out of the dPA monolayer.[58] The kink transition characteristic of dPA decreases from 25 mN/m to 22 mN/m in the dPA-BrPent mixed isotherm. This kink is a second order phase transition from the TC phase to the UC phase[46]. The dPA-BrPent film collapses at a surface pressure of 35 mN/m, which is lower than the collapse pressure of pure dPA. The collapse occurs at an MMA of 23 Å^2/molecule, whereas the dPA monolayer collapses at 20 Å^2/molecule. This difference suggests that even though some BrPent molecules are squeezed out of the dPA monolayer at low surface pressure, the film still contains both dPA and BrPent molecules.

The addition of BrHex (Figure 3.1b-3) and ClHex (Figure 3.1b-4) shifts the isotherm of pure dPA to larger areas at low surface pressures. BrHex has a greater effect than ClHex at low surface pressures. However, at high surface pressure ClHex seems to have a

27

slightly greater effect than BrHex. Previously, Gonçalves da Silva et al[36] showed similar effects of both BrHex and ClHex on heptadecanoic acid, whose alkyl chain is one carbon longer than that of dPA.

The dPA-BrHex isotherm lifts at 40 $Å^2$/molecule, whereas the dPA-ClHex isotherm lifts at 37 $Å^2$/molecule. The difference between dPA-ClHex and dPA-BrHex lift-off values can be partially explained by the difference in size of the halogen atoms where bromine is larger than chlorine, Br is 11.1 $Å^2$ and Cl is 6.8 $Å^2$. The surface pressure of both dPA-BrHex and dPA-ClHex isotherms rises significantly after the lift off. This region corresponds to the LC phase. Yet, the slopes of the LC phases in the mixed isotherms are smaller than that of the pure dPA.

The dPA-BrHex isotherm shows two collapse pressures. The initial collapse pressure appears at 16 mN/m, while the final collapse pressure at 37 mN/m is similar to that of pure dPA. This initial collapse pressure is attributed to the squeezing out of some BrHex molecules from the dPA monolayer as is discussed further with respect to the BAM images below. As the dPA-BrHex mixed monolayer is compressed further after the initial collapse pressure, there is an initial decrease in the slope of the isotherm, which suggests additional BrHex molecules are squeezed out. At the final collapse pressure, the dPA-BrHex isotherm is slightly shifted to higher MMA relative to that of the pure dPA indicating that a fraction of the BrHex molecules continues to be incorporated in the monolayer at this surface pressure.

Collapse pressure is defined as the highest pressure to which a monolayer cannot be further compressed without destabilizing the 2D nature of the monolayer and yielding 3D

structures due to the expulsion of molecules.[38,59] Collapse pressure has been used as a proof of miscibility or immiscibility of the components in a mixed monolayer at the air-water interface. When two fatty acids with different collapse pressures mix in a monolayer, the resulting isotherm might show a plateau at a pressure corresponding to the collapse pressure of the more fluid component (the component with the lowest collapse pressure) and a final collapse pressure similar to that of the more rigid component (the component with the highest surface pressure).[35,36,59] Thus, if the resulting isotherm of a mixed monolayer exhibits two distinct collapse pressures (initial and final), the different components of the monolayer have been identified as immiscible. On the other hand, if the resulting isotherm shows only one collapse pressure, the components are thought to form a homogeneous mixed monolayer. Here, even though two collapse pressures are observed, the isotherms are more complicated, and nonideal miscibility is suggested.

The isotherm obtained for the dPA-ClHex monolayer (Figure 3.1b-4) also shows two collapse pressures. The initial collapse pressure appears at higher surface pressures for the dPA-ClHex monolayer (19 mN/m) than for the dPA-BrHex system (17 mN/m). Contrary to the dPA-BrHex isotherm, the dPA-ClHex isotherm does not show a plateau upon further compression. However, the slope of the curve decreases similarly to the dPA-BrHex suggesting that ClHex molecules are being squeezed out of the dPA monolayer. The monolayer does not collapse exactly at the collapse pressure of the pure dPA, which suggests that the mixed monolayer continues to retain some of the ClHex molecules prior to and during the final collapse.

C_{15}, C_{16} Alkyl Halides, and dSA Mixed Monolayers. Figure 3.1c shows the surface pressure-area isotherms of dSA-BrPent, dSA-BrHex, and dSA-ClHex mixed monolayers on a pure water subphase with a mole ratio of 1:1. Similar to the effect on dPA, addition of BrPent, BrHex and ClHex shifts the pure dSA isotherm to larger areas, suggesting incorporation of the correspondent alkyl halide into the dSA monolayer.

For the mixed dSA-BrPent monolayer, the surface pressure-area isotherm (Figure 3.1c-2) consists of the same distinct regions from the pure dSA isotherm, TC and UC phases. The isotherm curve for this mixed monolayer is parallel to the pure dSA isotherm. Contrary to its effect on dPA, BrPent induces a relatively small shift to larger areas at low surface pressure on dSA monolayers. Upon compression, there is a transition from a G-TC to a TC phase at 28 $Å^2$/molecule. This lift-off value is far smaller than the lift-off value of the dPA-BrPent isotherm (57 $Å^2$/molecule). The slope of the TC region in Figure 3.1c-2 is comparable with that of pure dSA. The kink transition characteristic of dSA decreased from 27 mN/m to ~22.5 mN/m. As mentioned above, this kink corresponds to the transition from the TC phase to the UC phase. The dSA-BrPent film exhibits only one collapse pressure at ~39 mN/m. The fact that the surface pressure-area isotherm of dSA-BrPent is nearly parallel to the pure dSA isotherm and that it shows only one collapse pressure suggests the formation of a homogeneously mixed monolayer and miscibility with dSA. Thus, dSA incorporates BrPent into its monolayer to form a homogeneous and an apparently stable mixed monolayer, whereas dPA, being two carbons shorter ($C_{15}D_{31}COOH$) incorporates BrPent as well but the resulting mixed monolayer seems to organize differently with the BrPent molecules as seen from the very different phase

30

behavior. Hence, the length of the fatty acid plays a role in the extent of BrPent incorporation. However, both dSA and dPA are miscible with BrPent as suggested from the appearance of a single collapse pressure different from that of the dSA and dPA respectively.

Incorporation of BrHex and ClHex into dSA monolayers (Figure 3.1c-3 and 3.1c-4) follows a trend similar to the dPA monolayers. A difference observed for the BrHex and the ClHex mixed with dSA relative to the pure dSA is that their final collapse pressures are not at the same MMA. Both mixed isotherms collapse at a surface pressure ~10 mN/m lower than and at a MMA of ~2 Å^2/molecule larger than that of pure dSA. Two collapses are also observed for the mixed films with dSA as discussed above.

At collapse the isotherm pressures are shifted to larger MMA for the dSA mixtures relative to the dPA mixtures suggesting a difference in fractional composition. This could be due to the longer chain of dSA molecules which can favor lateral attraction with the chains of the alkyl halides thereby more efficiently retaining the alkyl halide in the film. One can also define this interaction as an indicator for miscibility.

Analysis of Figure 3.1b and 3.1c suggests that BrPent and 1:1 mole ratios of BrHex and ClHex are miscible with dPA and dSA, respectively. To further understand the miscibility of the RX molecules investigated here, we performed surface pressure-area isotherms at different mole ratios and the thermodynamic analysis (Appendix A). From this analysis, a nonideal miscibility between the alkyl halides and the fatty acids was concluded although the miscibility decreased with increasing surface pressure. Therefore,

the extent of miscibility is dependant on concentration within the monolayer and surface pressure.

3.2.2. SFG spectra

The normalized ssp and ppp SFG spectra of dPA and of the mixture dPA-BrHex 1:1 at the air-water interface at 5, 18, and 25 mN/m are shown in Figure 3.2 and 3.3, respectively. The ssp spectra taken in the C-D region to probe the dPA chains are shown in Figures 3.2a and 3.2b. The peaks present in the pure dPA (Figure 3.2a) spectra are attributed to the CD_3 symmetric stretch (ss; 2070 cm^{-1}), the CD_3 Fermi resonance (FR; 2125 cm^{-1}), and the CD_3 asymmetric stretch (as; 2220 cm^{-1}).[39,60] The ppp polarized spectral peak in Figure 3.3a-b is assigned to the CD_3-as (~2221 cm^{-1}). The dPA-BrHex SFG spectra (Figure 3.2b) are qualitatively similar to that of pure dPA. This is also true for the ppp SFG spectra shown in Figure 3.3a and 3.3b where only the methyl as is observed for the dPA and the BrHex. The appearance of dPA and BrHex peaks is confirmation that the BrHex molecules exist within the dPA monolayer.

The SF intensity of the CD peaks increases with surface pressure for both the pure dPA and the dPA-BrHex mixture as illustrated in Figure 3.4 by plotting the square root (proportional to number density) of the CD_3 ss SFG intensity of dPA. However, since SF intensity is a function of both number density and molecular orientation, the increase in intensity of the CD peaks is the result of a change in the number density of dPA molecules in the monolayer and/or a change in their orientation. To determine the cause of the increase in intensity, the average chain tilt angle (α) of dPA molecules with respect

to the surface normal was estimated. However, this calculation is only valid if the chains are in an all trans configuration according to SFG selection rules that require of lack of inversion symmetry for SFG activity. The absence of CD_2 peaks from the SFG spectra in Figure 3.2a-b indicates that the dPA molecules are in an all-trans configuration. Hence, the chain tilt angle was calculated according to previously established methods[61] by first determining the orientation angle (Θ) of the terminal methyl group from the SFG spectra by using the ratio of eq 3.1 to eq 3.2.

$$\chi_{ssp}^{(2)}(CD_3 - ss) = \frac{1}{2} N\beta_{ccc}[\cos\Theta(1+r) - \cos^3\Theta(1-r)] \tag{3.1}$$

$$\chi_{ssp}^{(2)}(CD_3 - as) = -N\beta_{caa}(\cos\Theta - \cos^3\Theta) \tag{3.2}$$

$\chi_{ssp}^{(2)}$ is the second-order nonlinear susceptibility of the CD_3-ss or CD_3-as vibration in the ssp polarization combination. $\chi_{ssp}^{(2)}$ is related to Θ, to the number density of interfacial molecules (N), and to the molecular hyperpolarizability (β). Here, r (β_{aac}/β_{ccc}) is taken as 2.3[62] and β_{caa}/β_{aac} as 4.2.[63] (Θ is sensitive to r and β_{caa}/β_{aac}; when changing r and β_{caa}/β_{aac} from 2.3 to 4.6 and from 4.2 to 2.1, the estimated angles would increase by ~8° and ~10°, respectively.) The ratio of $\chi_{ssp}^{(2)}(CD_3 - ss)$ to $\chi_{ssp}^{(2)}(CD_3 - as)$ is calculated to determine Θ. In practice, the ratio is calculated from the square root of the ratio of the experimental CD_3-ss to CD_3-as peak intensities. The calculated Θ and α are shown in

Table 3.2. α is calculated from the relationship between the C_3 axis of the terminal methyl. In an all-trans configuration, the C_3 axis of the terminal methyl group is at an angle of 35.5° from the axis of the alkyl chain. Therefore, the dPA chain tilt angle with respect to the surface normal can be estimated from the relationship $\alpha = 35.5° - \Theta$.[43,64]

The calculated chain tilt angle of dPA in a pure dPA monolayer is determined to be 18 ± 1° for the different surface pressures shown in Figure 3.2. Recall that at 5 and 18 mN/m, the dPA molecules are in the TC phase, and at 25 mN/m, the molecules transition from the TC phase to the UC phase. It is then expected that dPA molecules have a slightly different α at these surface pressures, with a decrease in angle for the UC phase. A significant change was not observed. Weidemann et al[65] determined by X-ray diffraction that the chains of PA at a pH of 2 were tilted by 25° at 10 mN/m, by 16° at 18 mN/m, and by 0° at 25 mN/m. In a different study[66] at 30 °C, a tilt angle of 21.4° at 15 mN/m and 5.3 at 30 mN/m were determined for PA. The pH was not stated in this study. In this study, the pH was ~6 in contrast to the pH of 2 from the Weideman et al study. PA has a surface pKa of ~8.5 and therefore the headgroup protonation state may have attributed to the different orientation angles. This study was conducted on pure water similar to the Lee study, however, the Lee study was conducted at 30° C, which also affects the pH of the subphase water. The calculated chain tilt angle of dPA in the dPA-BrHex mixed monolayer is determined to be 17 ± 1°. The small difference between the two systems, pure dPA discussed above versus the mixture, is within the error of the calculation. Therefore, it is concluded that the addition of BrHex does not affect the average value for the dPA chain tilt angle.

34

Since the difference in orientation angle as studied here is not significant between surface pressures in each system and between the pure dPA monolayer and the dPA-BrHex mixed monolayer systems, the change in SF intensity from dPA is directly correlated with a change in dPA number density. Therefore, from Figures 3.2a-b and 3.3a-b, the square root of the increase in ssp and ppp SF intensity with surface pressure should be directly proportional to the increase in dPA molecules as is shown in Figure 3.4. That is, as the monolayer is compressed, dPA molecules become more closely packed which results in more dPA per unit area probed. It can also be observed from Figures 3.2b and 3.3b that SF intensities are lower for the dPA-BrHex mixed monolayer than for the pure dPA monolayer. This is more evident at low surface pressures, suggesting that at low surface pressures BrHex molecules are incorporated into the mixed monolayer.

BrHex molecules were probed by acquiring ssp and ppp SFG spectra in the C-H stretching region of the mixed monolayer of dPA-BrHex 1:1 (Figure 3.2c and 3.3c respectively). The two main peaks observed in Figure 3.2c are attributed to the CH_3-ss (2872 cm^{-1}) and the CH_3-FR (2939 cm^{-1}). For Figure 3.3c, the single peak is assigned to the CH_3-as (~2963 cm^{-1}).[67-69] Contrary to the CD peaks from dPA molecules, the intensity of the CH peaks decrease as the monolayer is compressed.

3.2.3. IRRAS Spectroscopy

IRRAS spectra were obtained for two different systems, dPA-BrHex (3:1 and 1:1) and dSA-BrHex (3:1 and 1:1) to further elucidate conformational order, incorporation,

and BrHex number density. Due to differences in selection rules, IRRAS is sensitive to different vibrational modes of the fatty acids and alkyl halides compared to SFG and is therefore complementary to the SFG study above. Spectra of amphiphilic molecules show clear reflectance-absorbance peaks from the methylene groups of alkyl chains. The positions of the CH_2-ss and CH_2-as peaks are sensitive to the relative number of trans and gauche conformers, while the peak heights and areas indicate the packing density of the chains.

As control experiments, infrared transmission spectroscopy of the pure fatty acids (dPA and dSA) and the alkyl halides (BrPent, BrHex, and ClHex) were obtained and are shown in Figure 3.5a and 3.5b respectively. At 2087 and 2193 cm^{-1} in Figure 3.5a, the fatty acid CD_2-ss and CD_2-as modes are observed, and the peak at 1699 cm^{-1} corresponds to the C=O stretching vibration. In Figure 3.5b, the alkyl halide peaks at 2852 and 2923 cm^{-1} correspond to the CH_2-ss and CH_2-as modes, respectively.

In Figure 3.5c the s polarized IRRAS spectra of dPA and dSA monolayers on a water subphase at 25 mN/m are shown. Negative peaks are observed as expected. Both spectra show the CD_2-ss at 2087 cm^{-1}, the CD_2-as modes at 2193 cm^{-1} and the CD_3-as at 2216 cm^{-1}. Such frequencies for CD_2 vibrations are characteristic of transition moments perpendicular to the axis of an all-trans chain,[24] consistent with our interpretation from the SFG spectra above from the pure dPA monolayer in the UC phase. The IRRAS spectra also show structure around 1700 cm^{-1} formed by an upward-oriented band at 1650 cm^{-1} and a downward-oriented band at 1720 cm^{-1} (Figure 3.5c, inset I), which is assigned to C=O stretching vibrations. However, this band is formed by three peaks. Following

assignments made by Gericke and Hühnerfuss[44] for stearic acid, the peak at 1703 cm^{-1} is due to a doubly hydrated carbonyl group, the 1720 cm^{-1} peak is from the monohydrated state, and the 1737 cm^{-1} peak is due to the nonhydrated carbonyl group.[44,70] A 1088 cm^{-1} peak is observed (Figure 5c, inset II) and is assigned to the CD_2 scissoring mode.[24,71] The presence of this mode suggests a hexagonal or triclinic phase.[24,71,72]

IRRAS spectra of the dPA-BrHex 3:1 and 1:1 mixture are shown in Figure 3.6, and of dSA-BrHex 3:1 and 1:1 in Figure 3.7 at different surface pressures. In addition to the CD peaks observed at 2087 and 2193 2192 cm^{-1}, CH peaks from the BrHex are observed at 2852 and 2923 cm^{-1} which confirms that the BrHex molecules exist in the fatty acid monolayer as was also indicated by the SFG spectra from the dPA mixtures above. It is observed that as the surface pressure increases, the reflectance-absorbance intensity of the CD peaks increases. This is reasonable since upon compression, molecules become closer and therefore there are more molecules per unit area. On the other hand, CH peaks, which represent the alkyl halide molecules, decrease with surface pressure as was shown with the SFG data; however, we were able to obtain slightly enhanced signal intensities in these IRRAS spectra at the higher surface pressures. These results, IRRAS and SFG, are also consistent with the surface-pressure area isotherms and the area analysis that suggested that the alkyl halide molecules, although incorporated throughout the compression, are being squeezed out of the fatty acid monolayers as the compression proceeds. This is further shown in Figure 3.4, where the CD_2-as and CH_2-ss IRRAS intensity is plotted with the CD_3-ss and CH_3-ss SFG of dPA and BrHex respectively.

We also conclude from the IRRAS spectra that the alkyl chains of both fatty acids (dPA and dSA) increase in ordering with and without the BrHex as shown in Figure 3.8. The IRRAS BrHex frequency data did not show any trend in the mixed monolayers, which suggests that there is no discernable intermolecular interaction between the dPA and the BrHex alkyl chains, thus supporting the idea of miscibility.

Even though we observe a small red shifting of the dPA and dSA IRRAS CD_2-as frequencies as presented in Figure 3.8, the spectral range of the frequencies[24] supports predominately all-trans conformations at all surface pressures. This is also supported by the lack of SFG CD_2 peak intensities as shown in Figure 3.2 and as discussed above. The all-trans conformation of the fatty acids chains makes the dPA and dSA rigid molecules in their monolayers. It has been suggested that palmitic acid being a rigid molecule hinders the rotational isomerization of DPPC (dipalmitoylphosphatidylcholine) chains reducing the number of gauche defects, which forces DPPC molecules into a condensed phase.[39] In this investigation, the dPA and dSA effect on alkyl halide molecules may be similar to that on DPPC, forcing the alkyl halides into a condensed phase. As we mentioned above, contrary to their corresponding alkyl halides, alkanes do not incorporate into the fatty acid monolayers. Thus, in addition to having a relatively rigid fatty acid such as PA or SA, a head group that interacts with water is of great importance for formation of the monolayer.

Also, IRRAS spectra show that BrHex molecules are squeezed out with increase in surface pressure in accordance with the analysis of the isotherms and the MMAs as is suggested from Figure 3.4 as well. Fatty acid molecules force alkyl halide molecules into

38

a liquid or condensed phase in the mixed monolayer; however, the interactions of the fatty acid chains with the RX chains, and the halogen with water molecules are weak and therefore as the surface pressure increases, alkyl halide molecules are not retained in the monolayer. Contrary to the carboxylic acid headgroup that acts as a H-bond donor and acceptor during hydrogen bond formation with interfacial water molecules, a halogen can act only as an H-bond acceptor.[22]

The C=O stretching vibration band of both dPA-BrHex 1:1 and dSA-BrHex 3:1 shows the three peaks at 1737, 1720 and 1703 cm^{-1} (spectra not shown). The spectra also show the CD_2 scissoring mode at 1088 cm^{-1}. Comparing the spectra of the mixed monolayers with those of pure dPA and dSA, no frequency changes are observed, which suggests that the dPA and dSA conformation is not altered by the presence of BrHex. Ilharco et al.[58] investigated mixed Langmuir-Blodgett films of cadmium heptadecanoate with chloro/bromohexadecane on CaF_2 substrates by transmission IR. They observed a frequency shift of the COO^--as (at 1535 cm^{-1}) in the presence of alkyl halides. In our IRRAS spectra, the strong absorption of water vapor hinders the low spectral region from 1400 to 1600 cm^{-1} and therefore we were not able to observe this peak. Shifting of the COO^- peak could be indicative of miscibility of the alkyl halides and a changing environment for the fatty acid, and is not likely direct interaction with the halogen.

3.2.4. BAM Results

The isotherm, SFG, and IRRAS data clearly indicate that the long chain alkyl halides incorporate into mixed monolayer films of fatty acids. However, additional information

can be gleaned from surface images that provide organization information on a larger scale. Therefore, BAM images were obtained.

Three BAM images of pure BrHex after an attempt to spread on the water surface at varying compression are shown in Figure 3.9. The images are presented noting the average MMA; however, as shown in the isotherms of Figure 3.1a, BrHex, as well as the other RX molecules do not form monolayers at the air-water interface and therefore the surface pressure does not change with compression. As stated above, this is well known.[38] However, BAM images of BrHex provide an interesting contrast to the fatty acid and the mixed monolayer images shown in Figures 3.10 and 3.11. At 30 MMA and 27 MMA, the largest areas per molecule imaged, it is clear that monolayer spreading is not taking place and that aggregates of the BrHex are formed. The weave-like features are unique to the BrHex at the surface of water. At the smallest MMA of 14 MMA, the image shows larger areas of high reflectivity along with smaller and more reflective aggregates. The brightness indicates thicker films consistent with 3D structures as opposed to uniform 2D monolayer formation of dPA and dSA as discussed below. To our knowledge, this is the first published account of BAM images of alkyl halide molecules aggregating at the surface of water.

BAM images of pure dPA and its mixture with BrHex at different surface pressures are shown in Figure 3.10 to elucidate the 2D morphology changes of the mixed monolayers. In Figure 3.10a at 0 mN/m the darker background suggests either a pure water surface or a very low density of dPA molecules consistent with a 2D dPA G phase. The condensed phase is observed as round-shaped domains, which vary in size from a few microns to

hundreds of microns. Such domains show a uniform brightness indicating a uniform surface density and orientation of the alkyl chains consistent with a TC phase. Hence, these domains at 0 mN/m are attributed to the coexistence of the G phase with the TC phase. Upon film compression, the domains become closely packed and are more similar in size as shown in 3.10b. In 3.10c at 15 mN/m, a homogeneous film, which corresponds to the UC phase, is observed. (The periodic changes in the background intensity are discerned more obviously in images with homogeneous surfaces and are not attributed to structural changes in the films) The presence of a homogeneous film indicates that the alkyl chains in the dPA molecules have similar orientations and the film is of uniform thickness. These results are consistent with observations made by Qi et al[73] and Flach et al[74].

The surface pressure-area isotherms of dPA shift to the right when BrHex and dPA are mixed. The domains observed for pure dPA do not appear to be affected by the presence of BrHex as it is observed in the BAM images at low surface pressures in Figure 3.10d, e, g, and h. As the surface pressure is increased, a homogeneous film forms (Figure 3.10f and 3.10i). However, at 17.71 mN/m for the dPA-BrHex 3:1 (data not shown) and at 14.9 mN/m for the 1:1 mixture, aggregates with high reflectivity appear, similar to the small bright features observed in the BAM images of BrHex in Figure 3.9a and 3.9c. High reflectivity aggregates are indicative of multilayers. Since the SFG and IRRAS results suggested that BrHex molecules are squeezed out, and from the evidence from the BrHex images, these bright aggregates are likely comprised of BrHex molecules. This is

consistent with the BrHex surface pressure-area isotherm initial collapse at ~16 mN/m (Figure 3.1b-4), indicating some phase separation at those surface pressures.

The BAM images of dSA and its mixtures are presented in Figure 3.11 and are distinctly different than the dPA BAM images. Figure 3.11a shows the characteristic morphology of stearic acid at 0 mN/m.[75] The bright regions indicate higher densities of dSA molecules relative to the darker regions. Lee et al[75] suggested that the gas-phase forms elliptical domains and disperse in the condensed phase, as is observed in Figure 3.11a. Upon compression the high density dSA domains coalesce to form a uniform film as is observed in Figure 3.11b and 3.11c. In the case of dSA mixed monolayers, the same trend as with dPA is observed. The addition of BrHex does not significantly affect the dSA morphology. Figure 3.11d and 3.11g show the characteristic morphology of dSA at 0 mN/m. Upon compression of the mixed monolayers, highly reflective aggregates appear at 9.47 mN/ for dSA-BrHex 1:1, which is consistent with the initial collapse of its surface pressure-area isotherm (Figure 3.1c-3) and the squeezing out of a fraction of the alkyl halide molecules as aggregates.

From a surface area analysis of Figures 3.10 and 3.11, we have plotted in Figure 3.12 the surface area covered by domains.

To further examine the images relative to the respective isotherms of BrHex in the fatty acids, the fractional area of the bright domains obtained from the BAM images as a function of surface pressure was plotted in Figure 3.12. The fractional area of domains was estimated as the ratio of the area occupied by the domains in the BAM image to the total area of the BAM image and was obtained from these images in addition to

42

previously obtained BAM images. This analysis shows that upon comparison of the pure fatty acid films to the mixed films, an increase in area is occupied at a specified surface pressure, consistent with incorporation of the BrHex molecules into the monolayer. The large error bars observed for dPA at low surface pressures show that the dPA domains do not form a homogeneous film and that the density domain varies from low to high density. This is also observed for dSA at 0 mN/m. For the mixed monolayers, the area occupied by domains when the alkyl halide is present becomes larger at the same surface pressures. The MMA (in terms of area per molecule in the mixed monolayer not per fatty acid molecule) information obtained from the isotherms (Appendix A) suggests that it should decrease with addition of BrHex, however the BAM images show that the domains cover larger areas. This suggests that density in the mixed monolayer domains is lower compared to that of the pure fatty acid domains. The large area covered by mixed monolayer domains suggests that the molecules are in a more expanded conformation compared with the pure fatty acid domains.

3.3 Conclusions

Mixed monolayers of fatty acids and alkyl halides at the air-water interface were studied here by the combination of four complementary techniques, Langmuir isotherm measurements, SFG, IRRAS, and BAM. Alkyl halides, in contrast to long chain fatty acids, do not form monolayers by themselves at the air-water interface; however, organization of BrHex aggregates at the surface are observed by BAM. We determined that a chain length of 15 carbons for alkyl bromides is necessary for incorporation into

dPA and dSA monolayers. Contrary to this, alkanes do not incorporate into the fatty acid monolayers, indicating that even though the halogen is not a strongly polar group, it plays an important role for the incorporation of alkyl halides into fatty acid monolayers. Analysis of the surface pressure-area isotherms suggested that alkyl halide molecules are squeezed out of the fatty acid monolayers with increasing surface pressure, and BAM images confirm this. SFG and IRRAS results also revealed that alkyl halide molecules incorporate into the dPA and dSA monolayer, and that they are not retained as surface pressure increases. SFG and IRRAS spectra revealed that the alkyl chains of dPA retain a mostly all-trans conformation after the incorporation of alkyl halide molecules. Finally, BAM images reveal the miscibility of BrHex in dPA and dSA monolayers, and immiscibility at higher surface pressures as the BrHex multilayer aggregates are shown to be expelled at the first collapse pressure.

Table 3.1 Alkyl bromide molecules that are incorporated into fatty acid monolayers at the air-water interface at 1:1 ratio

	$C_{15}D_{31}COOH$ (dPA)	$C_{16}H_{33}COOH$ (HpA)	$C_{17}D_{35}COOH$ (dSA)
BrC_3H_7	No incorporation	No incorporation	No incorporation
BrC_4H_9	No incorporation	No incorporation	No incorporation
BrC_5H_{11}	No incorporation	No incorporation	No incorporation
BrC_6H_{13}	No incorporation	No incorporation	No incorporation
BrC_7H_{15}	No incorporation	No incorporation	No incorporation
BrC_8H_{17}	No incorporation	No incorporation	No incorporation
BrC_9H_{19}	No incorporation	No incorporation	No incorporation
$BrC_{10}H_{21}$	No incorporation	No incorporation	No incorporation
$BrC_{11}H_{23}$	No incorporation	No incorporation	No incorporation
$BrC_{12}H_{25}$	No incorporation	No incorporation	No incorporation
$BrC_{13}H_{27}$	No incorporation	No incorporation	No incorporation
$BrC_{14}H_{29}$	No incorporation	No incorporation	No incorporation
$BrC_{15}H_{31}$ (BrPent)	Incorporation	Incorporation	Incorporation
$BrC_{16}H_{33}$ (BrHex)	Incorporation	Incorporation	Incorporation

Table 3.2 Average orientation angle of the terminal methyl group (Θ) and average chain tilt angle (α) of dPA molecules in pure dPA monolayer and dPA-BrHex 1:1 mixed monolayer at different surface pressures

	Θ, CD$_3$ orientation angle (deg)	α, chain tilt angle (deg)
dPA 5 mN/m, TC	17.6 ± 1	17.9
dPA 18 mN/m, TC	17.4 ± 1	18.1
dPA 25 mN/m, UC	17.7 ± 1	17.8
dPA-BrHex (1:1) 5 mN/m	18.2 ± 1	17.3
dPA-BrHex (1:1) 18 mN/m	18.4 ± 1	17.1
dPA-BrHex (1:1) 25 mN/m	18.4 ± 1	17.1
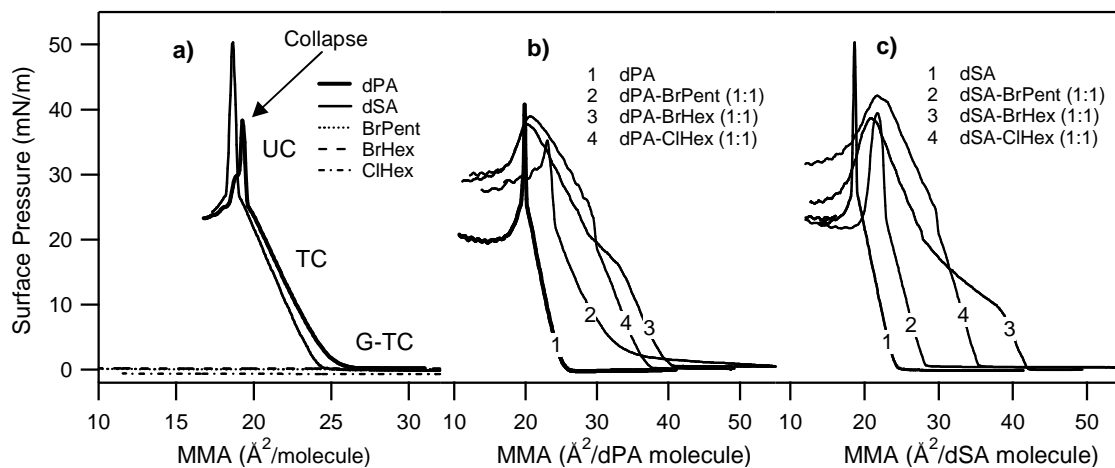
Figure 3.1 Surface pressure-area isotherms of a) pure compounds, b) dPA mixed monolayers and c) dSA mixed monolayers at the air-water interface. Mean molecular areas (MMA) of the mixed monolayers are in terms of number of fatty acid (dPA or dSA) molecules spread.
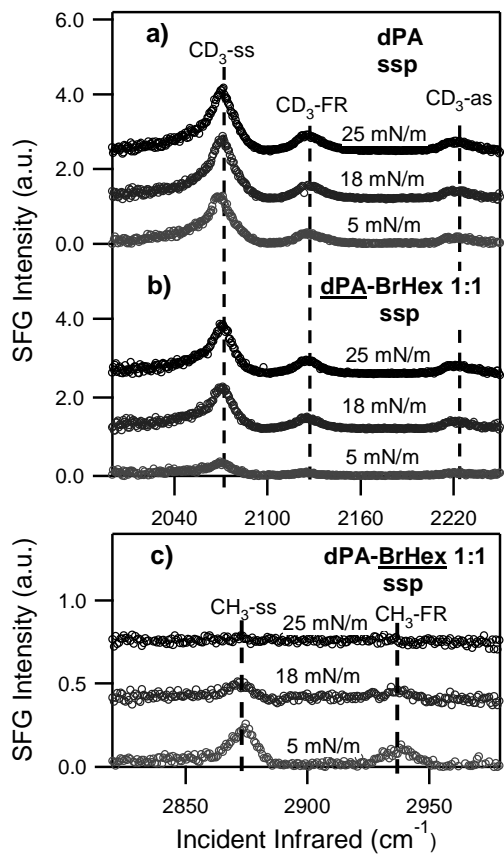
Figure 3.2 ssp SFG spectra probing dPA molecules in the CD stretching region of a) pure dPA and b) the mixture dPA-BrHex 1:1; and probing the BrHex molecules in the mixture dPA-BrHex 1:1 (c).
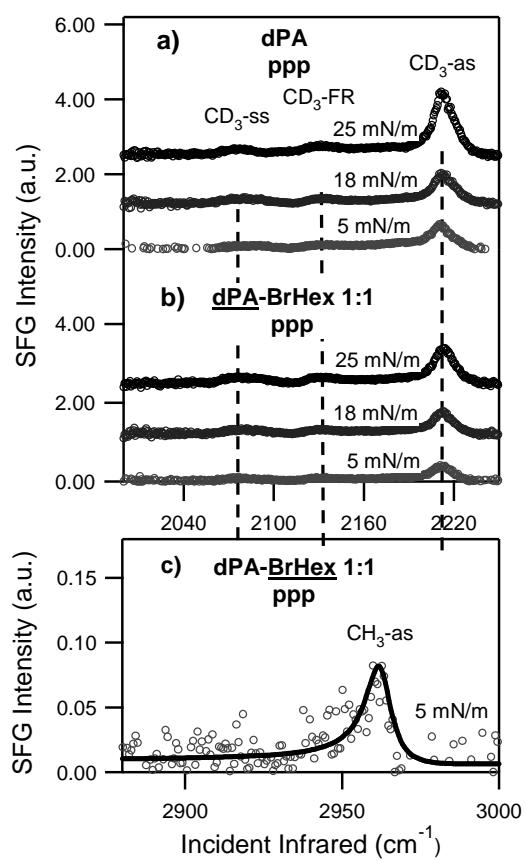
Figure 3.3 ppp BBSFG spectra probing dPA molecules in the CD stretching region of a) pure dPA and b) the mixture dPA-BrHex 1:1; and probing the BrHex molecules in the mixture dPA-BrHex 1:1 at 5 mN/m(c).
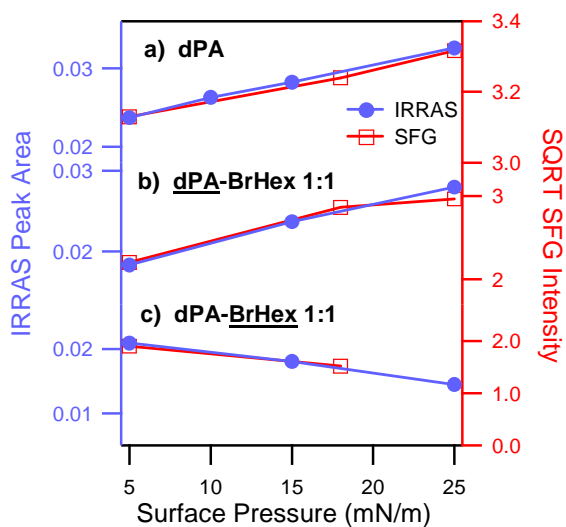
Figure 3.4 Comparison of the square root (SQRT) of the CD_3-ss peak intensity obtained by SFG and the CD_2-ss peak area obtained by IRRAS of dPA (a), dPA-BrHex 1:1 (b). Panel c) is the comparison of the SQRT of the CH_3-ss peak intensity obtained by SFG and the CH_2-ss peak area obtained by IRRAS of dPA-BrHex 1:1
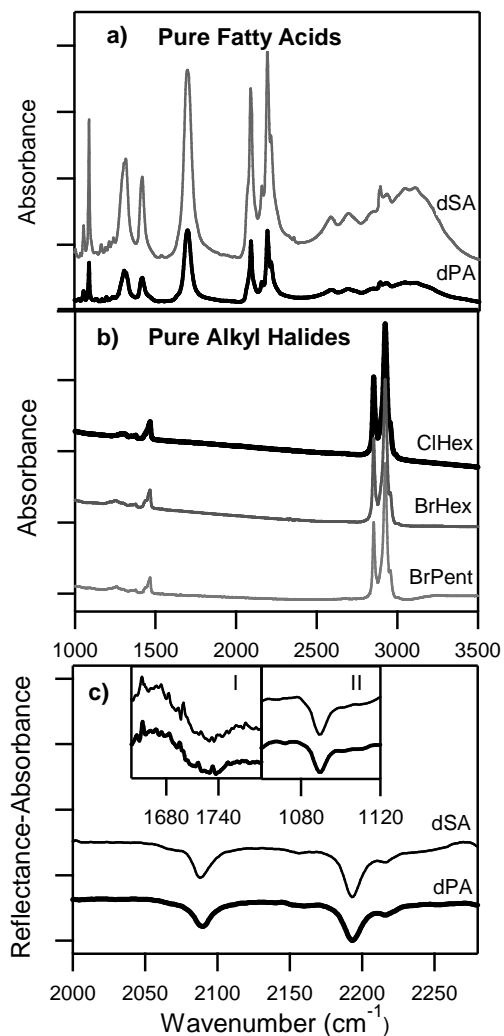
Figure 3.5 Absorbance infrared spectra of a) pure fatty acids and b) pure alkyl halides; and c) IRRAS spectra of pure fatty acids on a water subphase at 25 mN/m, spectra were collected with s polarized light. Inset I: C=O region. Inset II: CD_2 scissoring mode (1088 cm^{-1}).
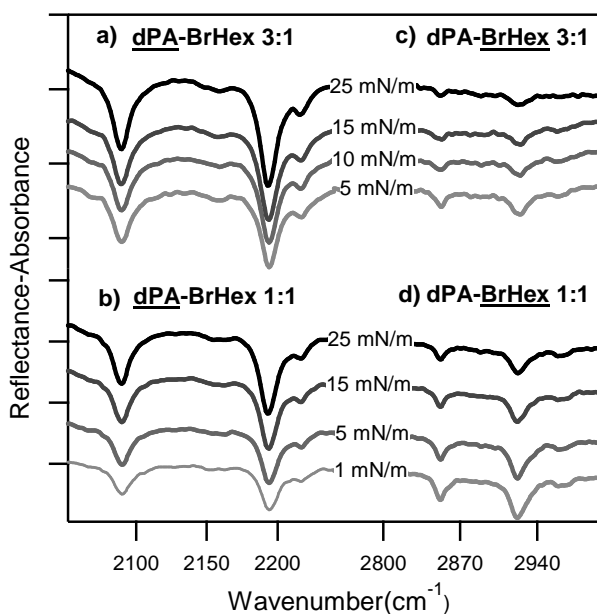
Figure 3.6 IRRAS spectra of the dPA-BrHex mixture at 1, 5, 15, and 25 mN/m obtained with s polarized light. Panels a (dPA-BrHex 3:1) and b (dPA-BrHex 1:1) show the CD stretching region, which represents the dPA component in the monolayer. Panels c (dPA-BrHex 3:1) and d (dPA-BrHex 1:1) show the CH stretching region, which represents the BrHex component in the monolayer.
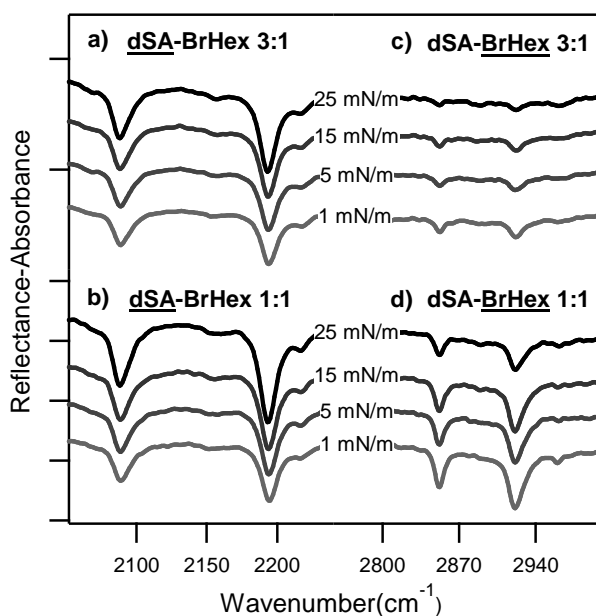
Figure 3.7 IRRAS spectra of the dSA-BrHex mixture at 1, 5, 15, and 25 mN/m obtained with s polarized light. Panels a (dSA-BrHex 3:1) and b (dSA-BrHex 1:1) show the CD stretching region, which represents the dPA component in the monolayer. Panels c (dSA-BrHex 3:1) and d (dSA-BrHex 1:1) show the CH stretching region, which represents the BrHex component in the monolayer.
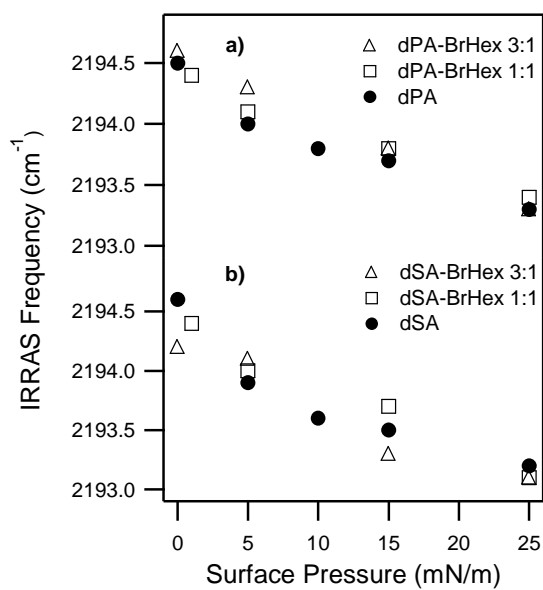
Figure 3.8. Frequency dependence of CD$_2$-as on the surface pressure of a) dPA and dPA-BrHex mixtures; and of b) dSA and dSA-BrHex mixtures

BrHex at 0mN/m

a

200 μm

30 Å^2/molecule

b

26 Å^2/molecule

c

14 Å^2/molecule
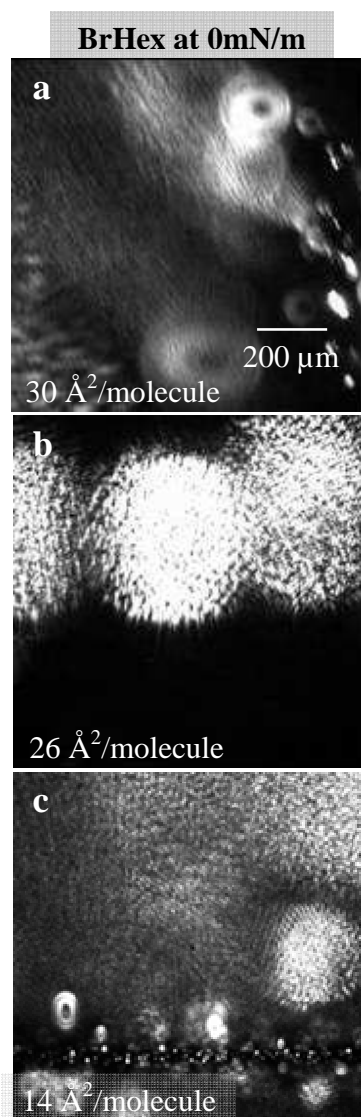
Figure 3.9. BAM images for pure BrHex at different MMAs.

dPA	dPA-BrHex 3:1	dPA-BrHex 1:1
a 100 μm 0 mN/m	**d** 0 mN/m	**g** 0 mN/m
b 5.0 mN/m	**e** 5.6 mN/m	**h** 5.41 mN/m
c 15.0 mN/m	**f** 14.23 mN/m	**i** 14.9 mN/m
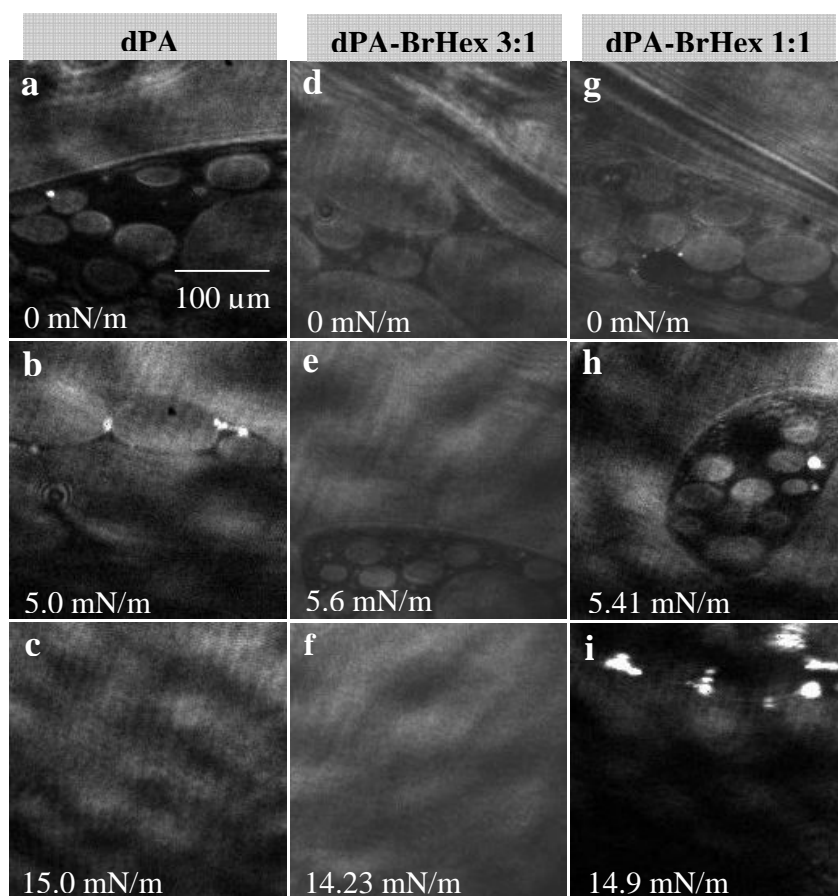
Figure 3.10 BAM images for pure dPA (a-c) for the mixed monolayer of dPA-BrHex 3:1 (d-f) and, for the mixed monolayer of dPA-BrHex 1:1 (g-i) acquired at different surface pressures
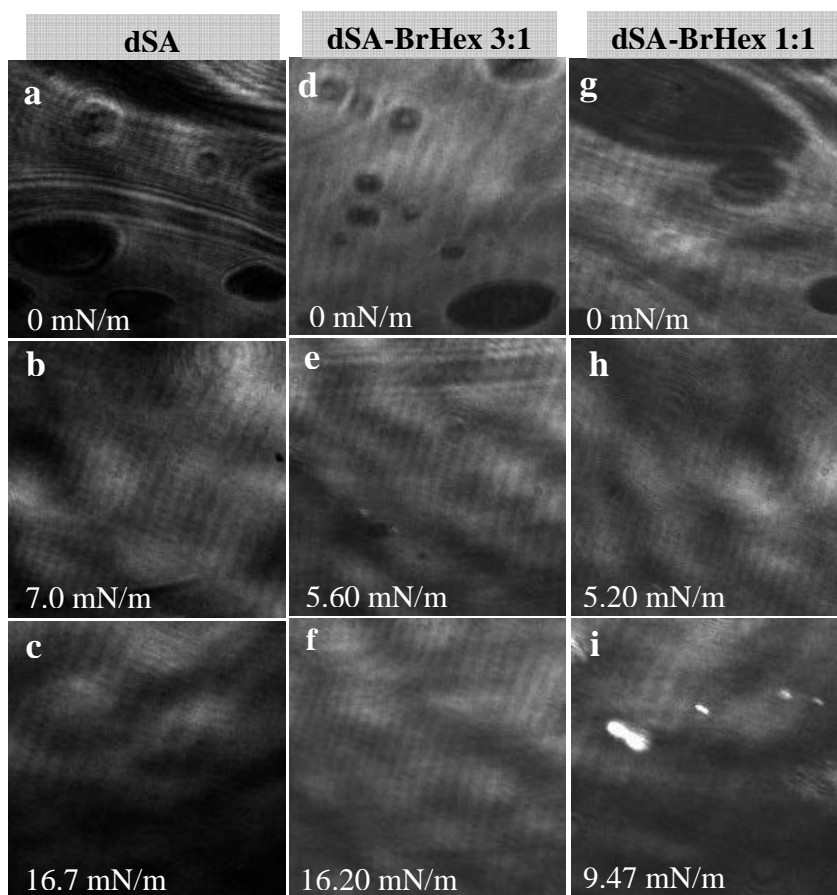
Figure 3.11 BAM images for pure dSA (a-c) for the mixed monolayer of dSA-BrHex 3:1 (d-f) and, for the mixed monolayer of dSA-BrHex 1:1 (g-i) acquired at different surface pressures
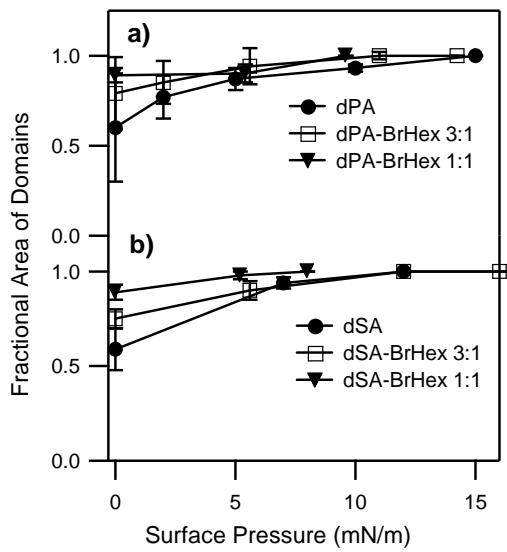
Figure 3.12 Fractional area of domains from the BAM images as a function of surface pressure for a) dPA and dPA mixtures, and for b) dSA and dSA mixtures

Chapter 4

Alkyl Halide and Alcohol Uptake at the Air-Water Interface

Halogenated organic compounds from both biogenic and anthropogenic sources are emitted to the atmosphere. Of the alkyl halides, short-chain alkyl halides have been found in the atmosphere. These include methyl chloride (CH_3Cl),[49,50] methyl bromide (CH_3Br),[8] methyl iodide (CH_3I), ethyl iodide (C_2H_5I), and 1-propyl iodide (C_3H_7I),[52] as well as CH_3CCl_3, CH_2Cl_2, and $CH_xCl_yBr_z$ among others.[8,53]

We studied in collaboration with Harper et al[22] the surface residence and organization of gas-phase methyl chloride (CH_3Cl), butyl chloride (C_4H_9Cl), and butyl bromide (C_4H_9Br) and their corresponding alcohol molecules adsorbed to the air-water interface. First, the adsorption of the gas-phase species to an aqueous surface was investigated by using vibrational sum frequency generation spectroscopy (VSFG). Then, their uptake into the bulk aqueous solutions was measured using Raman spectroscopy.

Previously, Harper[76] presented in her MSc thesis VSFG spectra of the gas-phase species at the air-water interface using ssp polarization combination. Additionally, her thesis includes Raman spectra of the water solution exposed to CH_3Cl and CH_3OH. Later, Casillas-Ituarte[77] presented in her PhD dissertation VSFG spectra of the gas-phase species at the air-water interface using ssp, ppp, and sps polarization combinations.

Additionally, Raman spectra of all the gas-phase species into the bulk aqueous solutions were shown.

Our findings revealed the presence of CH_3OH at the air-water interface and in the bulk aqueous solutions. Contrary to the CH_3OH, CH_3Cl was not detected at the air-water interface. However, CH_3Cl was detected in the bulk aqueous solution indicating that CH_3Cl gas-phase molecules must interact with the air-water interface so that their uptake into the aqueous phase occurs. The same trend was observed for the butyl species as was observed for the methyl species. The butyl alcohol (C_4H_9OH) was detected at the air-water interface whereas the butyl halide species were not detected.[76] It was shown that although C_4H_9OH was detected in the aqueous phase, the butyl halide species were not detected, which may be due to their low water solubility.[77]

The lack of alkyl halide VSFG signal at the air-water interface suggests that such gas-phase species are not adsorbed at the interface. However, other possible reasons such as low number density, disordered interfacial arrangement, short surface residence time, infrared (IR) absorption by the gas-phase species or some combination of them must be further investigated.

To determine if IR absorption by the gas-phase species was a factor for the lack of alkyl halide VSFG signal, we measured the IR energy coming out of the experimental chamber using a scanning SFG (SSFG). The results obtained showed that the lowest IR energy measurement was obtained after flowing CH_3OH. These results suggested that the IR energy for the alkyl halide VSFG experiments was sufficient to generate sum frequency signal.[77]

The gas phase concentration of CH_3OH and CH_3Cl, which was measured to determine if gas phase concentration was a factor that contributed to the VSFG lack of signal, is presented here. Additionally, the concentration of CH_3OH in the aqueous phase of the flow experiments is shown in this chapter.

4.1 Experimental

4.1.1 Materials

Methyl alcohol (CH_3OH; HPLC grade), n-butyl chloride (C_4H_9Cl; ACS certified), and n-butyl alcohol (C_4H_9OH; ACS certified) were obtained from Fisher Scientific. n-Butyl bromide (C_4H_9Br; 99+% purity) was obtained from Acros Organics. Methyl chloride (CH_3Cl; 99.5% purity, instrument grade) was obtained from Scott Specialty Gases, Inc. (Plumsteadville, PA). Nitrogen (N_2) was obtained from Praxair, Inc. (Danbury, CT). Deionized water with a resistivity of 18.2 MΩ·cm was used (Barnstead Nanopure filtration system). All experiments were conducted at room temperature (21°C ± 1°C).

4.1.2 Methods

The flow of the gas-phase species was performed in a flow chamber comprised of a stainless steel lid that attaches to a stainless steel cylindrical base by using a knife-edge sealing technology in conjunction with a copper gasket. The incident beam(s) enters the chamber through a BaF_2 window (Reflex Analytical Corp., p/n 8960-1BAF2) and the outcoming beam (SFG or IR) exits the chamber through a BK7 window (Kurt J. Lesker Co., p/n VPZL-275BK7) (Figure 4.1).

The gas phase concentration of CH_3OH and CH_3Cl was determined by using a Thermo Nicolet FTIR (Fourier transform infrared) spectrometer (Avatar 370, Thermo Electron Corporation). The IR beam was directed out of the compartment of the FTIR spectrometer with a series of gold flat mirrors to the flow chamber. The flow chamber contained a gold mirror to redirect the IR beam out of it. The IR beam coming out of the flow chamber was then directed back to the detector of the FTIR spectrometer (Figure 4.2). CH_3OH was volatilized by flowing nitrogen gas (N_2) at 15 standard cm^3/min (sccm) through the liquid CH_3OH contained in a glass vial. The resulting N_2/CH_3OH mixture was flowed over 24 mL of water contained in a Petri dish in the flow chamber. CH_3Cl on the other hand, having a high vapor pressure was flowed directly from its pressurized tank at 10 sccm. The flow conditions for each compound were kept the same as described for the surface analyses completed with the BBSFG system.[22,76] Spectra were collected every 5 minutes at a resolution of 4 cm^{-1} and averaged over 50 scans for 120 minutes. To determine the gas-phase concentration of CH_3OH, it was first necessary to estimate experimentally the extinction coefficient at 2875 cm^{-1}.

A 22-cm tube was placed between the windows of the FTIR spectrometer. N_2/CH_3OH and CH_3Cl were flowed into the 22-cm tube at the flow rates mentioned above. Spectra were collected every 5 minutes at a resolution of 4 cm^{-1} and averaged over 50 scans for 90 minutes. The gas phase concentration in the 22 cm-tube was determined by using the absorbance of the CO-ss at 1052 cm^{-1}. A cross section of 1.388 x 10^{-20} cm^2/molecule reported on HITRAN data base was used.[78] The concentration was used to construct a calibration curve for the 2875 cm^{-1} absorbance peak as a function of concentration. The

slope of the curve corresponds to the extinction coefficient at 2875 cm^{-1}. The concentration of CH_3Cl was estimated by using the absorbance of the CH_3-ss at 2922 cm^{-1} [78].

The concentration of CH_3OH in the aqueous phase of the flow experiments was determined by ATR-FTIR (attenuated total reflection FTIR). A multi bounce ZnSe crystal trough ATR accessory was used to collect the spectra at a resolution of 4 cm^{-1}. The spectra were averaged over 200 scans. A calibration curve of CH_3OH in aqueous solutions was obtained by using the absorbance of the CO-ss at 1052 cm^{-1}. The CH_3OH concentration was determined at 30, 60, and 120 minutes of flow.

The number of molecules flowed to the chamber was measured by weighting the glass vial containing the CH_3OH before and after the flowing.

4.2 Results and Discussion

The CH_3OH and CH_3Cl concentrations are shown in Figure 4.3. The CH_3OH and CH_3Cl concentrations after two hours were determined to be 4.16 x 10^{17} and 1.17 x 10^{19} molecules/cm^3, respectively. These results show that the CH_3Cl gas-phase concentration was two orders of magnitude greater than that of CH_3OH, and therefore the gas-phase concentration was not a limiting condition for the lack of SFG signal of CH_3Cl.

The gas phase concentration of CH_3OH measured with the FTIR is compared in Figure 5.4 with the square root of the SFG intensity of the 2835 cm^{-1} peak. The square root of the SFG intensity is proportional to the number density of molecules at the air-water interface. It is observed from Figure 4.4 that the CH_3OH gas phase concentration and its

63

number density at the air-water interface increase quickly during the first 10 minutes of CH_3OH flow. After 40 minutes of CH_3OH flow, the number of CH_3OH molecules at the gas phase and at the air-water interface is at equilibrium. This finding indicates that the time to monitor the adsorption of CH_3OH to the aqueous surface was long enough. This result can be extrapolated to the CH_3Cl gas-phase result observed in Figure 4.3. After 60 minutes of CH_3Cl flow, the gas-phase concentration is relatively constant and therefore it is assumed that it is at equilibrium. Thus, the time to monitor CH_3Cl adsorption to the aqueous surface was assumed to be long enough as well. Therefore, the length of the CH_3Cl experiment did not limit for the SFG signal of CH_3Cl.

A calibration curve of CH_3OH in aqueous solutions was obtained to determine the CH_3OH concentration in the aqueous solutions of the flow experiments, and it is shown in Figure 4.5. The CH_3OH concentrations in the aqueous phase of the flow experiments are shown in Table 4.1. The concentration increased linearly with time, which was expected since CH_3OH is soluble in water.

The number of molecules flowed to the chamber was measured by weighting the glass vial containing the CH_3OH before and after the flowing. The weight difference was used to calculate the total number of molecules flowed into the chamber and is shown in Table 4.2. During the flow, molecules diffuse into the 24 mL of water (number calculated from the calibration curve, third column in Table 4.2), while others stay in the gas phase. The number of molecules in the water added to the number of molecules in the gas phase after 30 min of flow was 1.79×10^{21} molecules/cm^3, which is ~ 85% of the number of molecules calculated by weight loss. This suggests that the other 15% of the molecules

are adsorbed at the water interface. The summation of the number of molecules in the water and in the gas phase after 60 and 120 min of flow are 3.10×10^{21} and 6.53×10^{21} molecules/cm^3 respectively. These two values represent 60% and 70% from the total number of molecules flowed, suggesting that water surface is becoming saturated by CH_3OH molecules and that the system is at equilibrium.

4.3 Conclusions

Adsorption of gas-phase alkyl halides and alcohols to the air-water interface was previously studied using surface sensitive vibrational sum frequency spectroscopy. We showed in previous publications[22] that CH_3OH is present at the air-water interface and in the bulk aqueous solutions, whereas CH_3Cl was only found in the bulk. Here, the gas phase concentration of CH_3OH and CH_3Cl was measured to determine its possible contribution for the lack of VSFG signal for CH_3Cl. Our findings revealed that the number of CH_3Cl molecules in the gas phase was larger than the number of gas phase CH_3OH molecules and therefore it is not a factor for the lack of VSFG signal. The length of the experiment was tested to determine if it was a factor for the lack of VSFG signal for CH_3Cl. The results showed that the systems were at equilibrium. Therefore, the length of the CH_3Cl experiment was not a limiting for the lack of SFG signal of CH_3Cl. The results previously published and those of this chapter suggest that orientation (disordered molecules) and low number density explain the absence of the CH_3Cl signal in the SFG spectrum.

Table 4.1 Bulk CH_3OH concentration of flow experiments. St. Dev is the standard deviation of two repetitions

Time (minutes)	CH_3OH Concentration (M)	St. Dev.
30	0.11	0.007
60	0.19	0.016
120	0.45	0.014

Table 4.2 Number of CH_3OH in the flow chamber. The total number of molecules represent the number of molecules flowed into the chamber calculated by weight loss. Number of molecules in the 24 mL of water was calculated from the calibration curve. Number of molecules in the gas phase was measured by FTIR

Time (minutes)	Total number of molecules	Number of molecules in 24 ml of water	Number of molecules in the gas phase
30	2.06×10^{21}	1.71×10^{21}	3.10×10^{17}
60	5.21×10^{21}	3.01×10^{21}	3.37×10^{17}
120	9.12×10^{21}	6.04×10^{21}	3.92×10^{17}
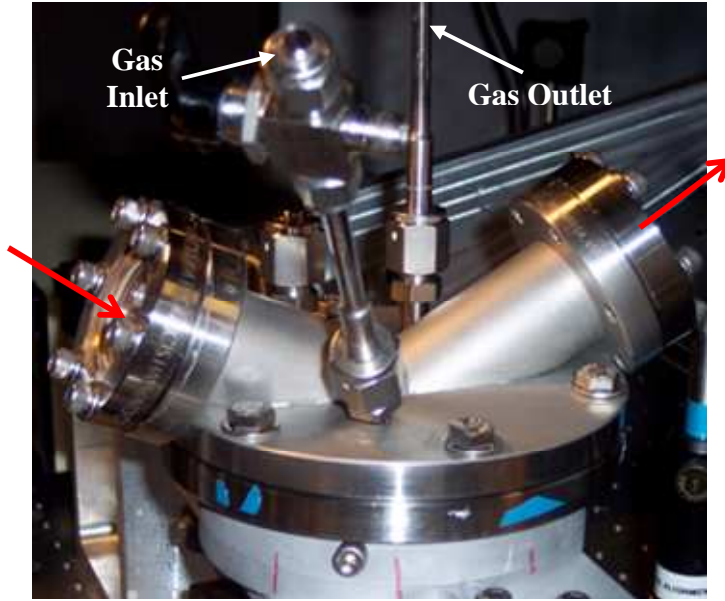
Figure 4.1 Flow chamber comprised of a stainless steel lid that attaches to a stainless steel cylindrical base by using a knife-edge sealing technology in conjunction with a copper gasket. The incident beam(s) enters the chamber through a BaF_2 window and the outcoming beam (SFG or IR) exits the chamber through a BK7 window.
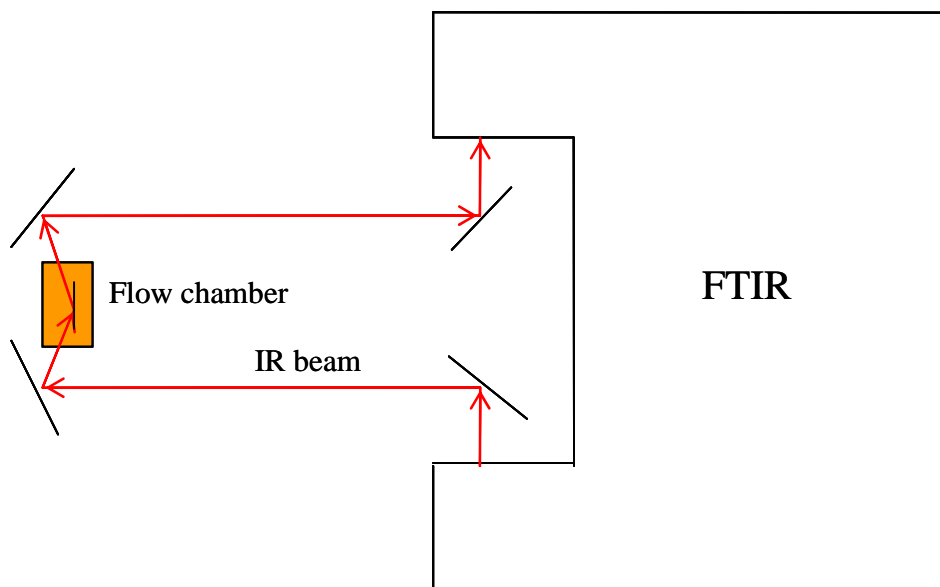
Figure 4.2 Experiment set up for the determination of the gas-phase concentration using the FTIR
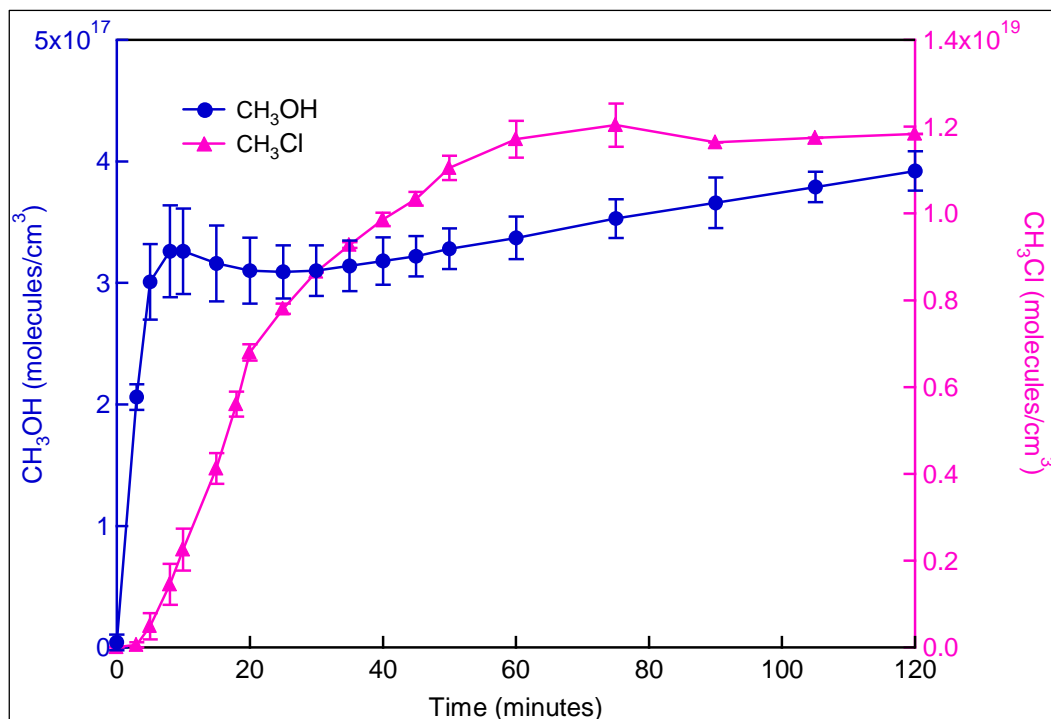
Figure 4.3 Gas phase concentration of CH_3OH and CH_3Cl measured by FTIR over time
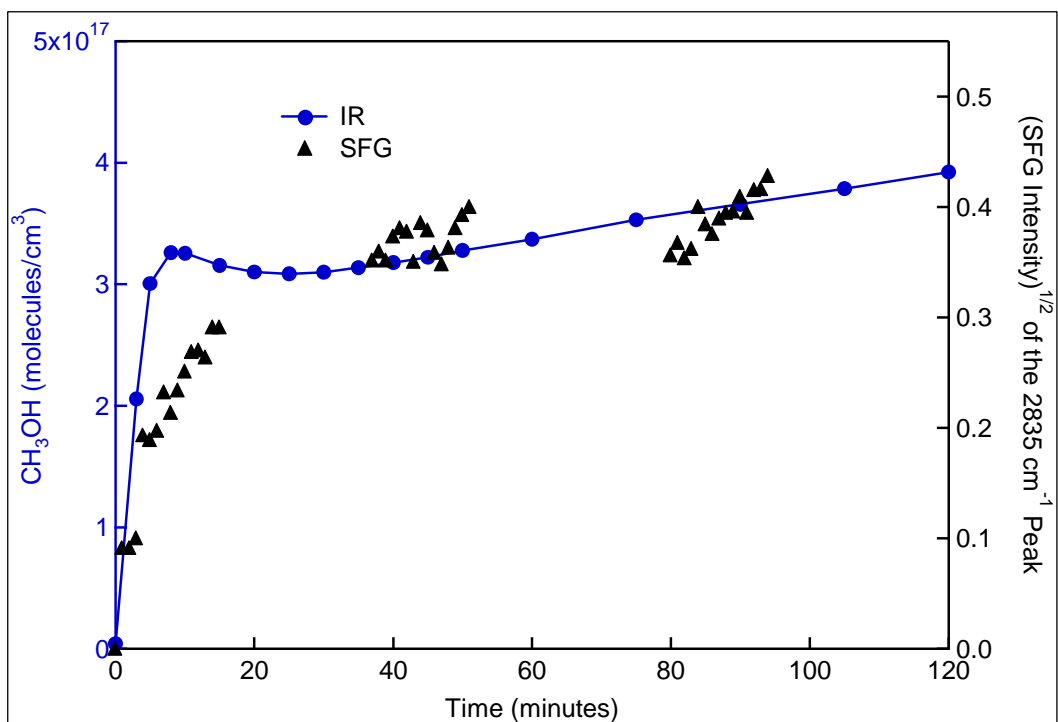
Figure 4.4 Gas phase concentration of CH$_3$OH over time compared to the square root of the SFG intensity of the 2835 cm^{-1} peak
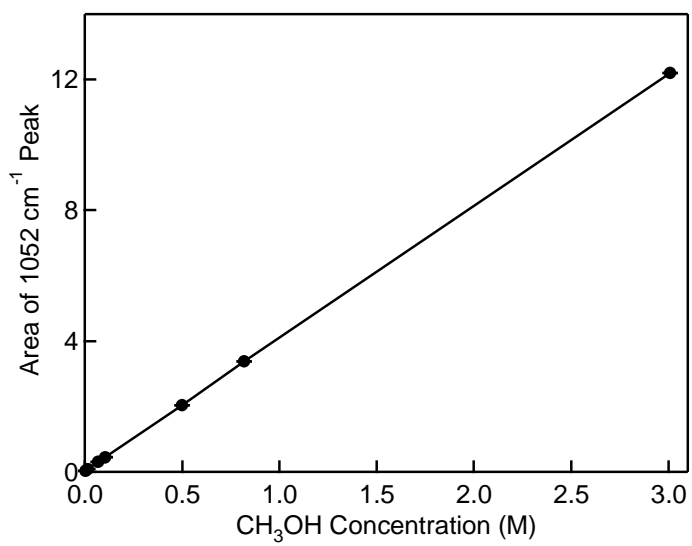
Figure 4.5 Calibration curve of CH₃OH in aqueous solutions

Chapter 5

Air-Aqueous Acid Interfaces

The chemistry of atmospheric aerosol surfaces plays a critical role in the uptake of gas-phase chemical species and in their reactions.[8] Therefore it is important to investigate the identity and orientation of these species at the surface of atmospheric aerosols. A molecular-level understanding of air-aqueous interfaces is a fundamental study that will help us understand atmospheric aerosol surfaces.

The effect of halide ions[79,80] and protons[80] has been studied previously in our research group. Levering[80] studied the effect of hydrogen halides (hydrochloric, hydrobromic and hydroiodic acids, HCl, HBr, and HI, respectively) at the air-water interface using vibrational sum frequency generation spectroscopy (VSFG). In this study, it was found that HCl, HBr, and HI disrupt the hydrogen-bonding network at the air-liquid interface. This was observed by an enhancement of intensity in the water OH stretching modes. It was also observed that the free OH intensity decreased with all acids tested. In this study, the authors used a 10Hz scanning system,[79,80] which provides spectra in the 2800 – 4000 cm^{-1} range. In this chapter, spectra at lower frequencies of neat water, sodium bromide (NaBr) and HBr are presented. Lower frequencies were investigated to further explore the enhanced intensity of the OH stretching region by using a 20 Hz scanning VSFG

system that provides spectra. Additionally, to determine if the free OH peak decrease is due to a change in number density or a change in orientation, the VSFG spectra of two different HBr aqueous solutions in the free OH region are presented in this chapter under ssp and ppp polarization combinations.

5.1 Experimental

5.1.1 Materials

Water was obtained from a Millipore Nanopure system (18.3 MΩ•cm). Acid solutions were made volumetrically from concentrated HBr (Fisher Scientific, 48 % wt.) solution. Sodium bromide salt (certified ACS grade) was purchased from Fisher Scientific. The NaBr salt was baked in a muffle furnace (Fisher Isotemp) for 6 h at 650°C to eliminate organic contaminants. All of the solutions were checked for organic contamination by obtaining SFG spectra of the solutions in the spectral region between 2800 and 3000 cm^{-1}.

5.1.2 Methods

SFG spectra were acquired using the 20 Hz scanning VSFG system from EKSPLA. The ssp-polarized SFG spectra were acquired using a 15 s exposure time for each data point and are an average of two spectra. The SFG spectra were normalized by the IR profile since the IR is detected in real-time with the SFG intensity. An SFG spectrum of an 8.0 mM sodium dodecyl sulfate (SDS) solution was acquired at the beginning of each experiment day to optimize the overlap of the visible and IR beam at 2940 cm^{-1}. Additionally, at least one air-neat water spectrum was acquired at the beginning and at

the end of each experiment day to ensure the stability of the SFG system and to confirm reproducibility. The polarization combination used for these experiments was ssp (SFG, 532 nm, and infrared beams respectively).

SFG spectra of neat water and HBr aqueous solutions in the free OH region (3600 – 3800 cm^{-1}) were acquired with the BBSFG system. The BBSFG system is described in Chapter 2. Here, the angles of the infrared and visible beam (789.5 cm^{-1}) from the surface normal were 68° and 53°, respectively. The input energy of the visible beam was 300 µJ whereas the infrared energy was of 6 µJ. SFG spectra were normalized to the nonresonant signal from a GaAs crystal. The spectra were obtained under the ssp and ppp polarization combinations with an acquisition time of 3 minutes. An average of two replicate spectra is shown for each solution and the error bars represent the standard deviation between them.

5.2 Results and Discussion

The raw SDS spectrum acquired as a control on each experimental day is shown in figure 5.1. The intensity signal required for the 2940 cm^{-1} peak to determine that the SFG system was in optimal conditions was approximately 740 counts as it is shown in Figure 5.1.

The VSFG spectra of neat water in the range of 2800 – 3800 cm^{-1} is shown in Figure 5.2. The spectra show a broad continuum from 3000 cm-1 to 3600 cm^{-1} which has been assigned to the OH stretching bands of hydrogen-bonded water molecules.[79,81-83] At 3700

cm^{-1}, not part of the continuum, a narrow peak which is attributed to the dangling OH (free OH directed into the vapor phase) is observed.

VSFG spectra of neat water, 0.050x NaBr, and 0.050x HBr (Figure 5.3) were acquired to explore the enhanced intensity of the OH stretching region in the VSFG spectra of aqueous acid solutions. Additionally these spectra would provide further support for the existence of H_3O^+ and $H_5O_2^+$ in the interface at frequencies lower than 2800 cm^{-1}. As shown in Figure 5.3, the VSFG spectra of aqueous NaBr solution have no enhanced intensity at frequencies in the range of 2000 – 3200 cm^{-1} as compared to that for neat water. On the other hand, the aqueous HBr solution VSFG spectra clearly show a significant intensity enhancement of the hydrogen-bonded stretching region (2400 – 3200 cm^{-1}) and a decrease of the free OH peak intensity when compared to both aqueous NaBr and neat water. Spectral backgrounds on the same samples with the timing of the pulses offset, as are typically done for our control experiments, are shown as open circles. The observed VSFG enhancement is consistent with the observed enhancements in IR and Raman spectra,[82] that is, the proton continuum. This continuum clearly indicates that H_3O^+ (and/or $H_5O_2^+$) exists within the air-aqueous acid interface.[82] Enhancement of the 3200 cm^{-1} region is most likely due to the presence of hydronium ions at the air-aqueous interface. This is consistent with previous experimental studies[84-86] and molecular dynamic simulations.[84,87] This important result clearly lays to rest the question of hydrated protons in the interfacial region.

Previous investigations have inferred the presence of the hydronium at the air-water interface as discussed below. Petersen and Saykally[85] have clearly shown that iodide ions

are enhanced at the air-water interface in aqueous HI as opposed to aqueous KI and NaI, inferring that the hydronium is surface active and thereby allowing the iodide anions to be more surface active relative to the aqueous KI and NaI surfaces. Jungwirth, Tobias, Allen and coworkers[84] postulate through MD simulation and VSFG data that hydronium exists in the interfacial region. Richmond and coworkers[86] also strongly suggest that hydronium resides in the surface region of aqueous halogen acid solutions. With respect to surface H_3O^+, Lee and coworkers[88] observed the gas phase infrared spectra of the hydrated hydronium cluster ions $H_3O^+ \bullet (H_2O)_n$ (n = 1, 2, 3) from 3550 to 3800 cm^{-1}. Two features were visible for $H_5O_2^+$: a broad, featureless band at 3608.8 cm^{-1} and a higher frequency band centered at 3684.4 cm^{-1}. Graham and Roberts[89] have also examined the infrared spectrum of the HCl $\bullet$ 6H_2O complex; vibrational modes centered at 1770 and 1275 cm^{-1} and the broad peak between 2500 and 3100 cm^{-1} were assigned to the ν_4, ν_2, and ν_3 modes of H_3O^+, respectively. Scherer, Voth and coworkers[90] investigated the infrared spectra of HCl and HBr aqueous solutions and observed a continuous absorption from 1000 to 3400 cm^{-1} and three broad bands at 1760, 2900, and 3350 cm^{-1}, which are attributed to the hydrated proton.

In summary, the proton continuum observed in Figure 5.3 provides strong evidence for the existence of hydrated protons (H_3O^+ and $H_5O_2^+$) within the air-aqueous acid interface. The VSFG spectra of HBr also reveal a decrease in the 3700 cm^{-1} peak (free OH stretch) intensity relative to neat water as shown in Figure 5.3. To determine if this is due to a change in number density or a change in orientation, the VSFG spectra of two different HBr aqueous solutions in the free OH region were acquired under ssp and ppp

77

polarization combinations (Figure 5.4). The spectra reveal that the ratio of the ssp to the ppp intensity in the free OH peak is relatively constant for two different aqueous HBr concentrations.

According to previous studies,[91,92] the orientation fluctuation of the free OH oscillator may occur in a time scale that could match its vibrational relaxation time or even shorter. Reorientation affects the SFG intensity response if reorientation is fast. [92] However, this effect is relatively modest under the ssp and ppp polarization conditions. Moreover, in addition to the fast reorientation motion effect, the applied orientation angle distribution can also affect the SFG intensity response. Wang and coworkers[91,93] determined the average orientation angle of the free OH oscillator on the neat water surface to be 33° with respect to the surface normal with a constrained orientation distribution less than 15° assuming a Gaussian distribution. In order to fulfill the same degree of intensity loss found in the spectra, the orientation angle distribution has to encompass a much wider spread, which is physically unreasonable. This is consistent with an intensity decrease due to a number density decrease of free OH oscillators at the surface and not a change of orientation angle and/or orientation angle distribution width.

5.3 Conclusions

The air-aqueous interface of aqueous HBr and NaBr solutions was investigated using vibrational sum frequency generation spectroscopy. Enhanced intensity was observed in the water OH stretching modes of the HBr solutions. The SFG spectra reveal a surface

proton continuum at frequencies below 3000 cm^{-1}, indicating that hydronium ions and Zundel ions (H_3O^+ and H_5O^{2+}) exist at the air-water interface.
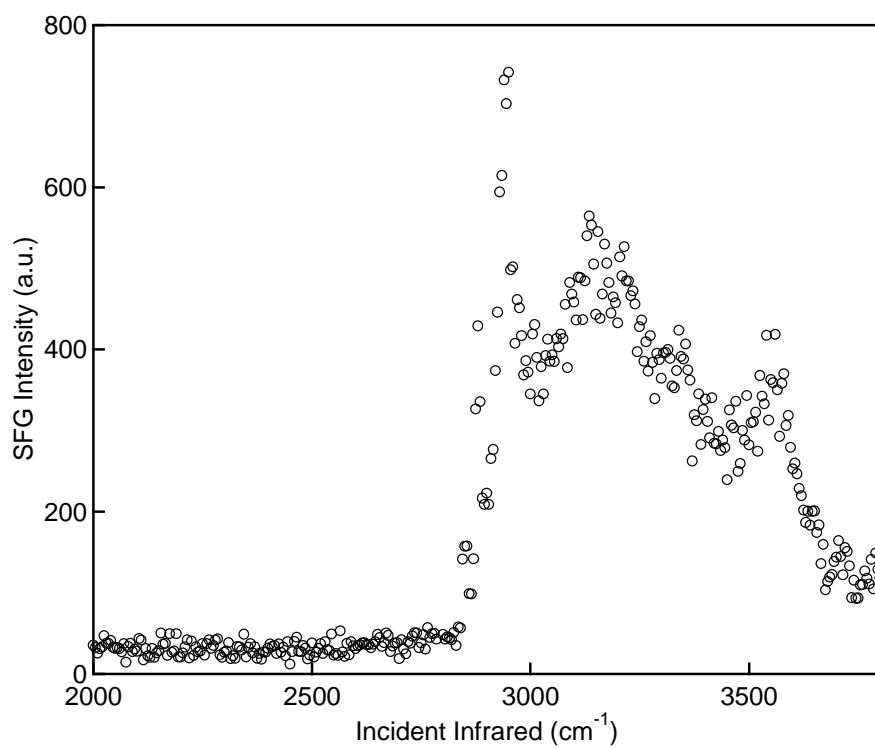
Figure 5.1 ssp VSFG raw spectrum of an 8.0 mM SDS solution.
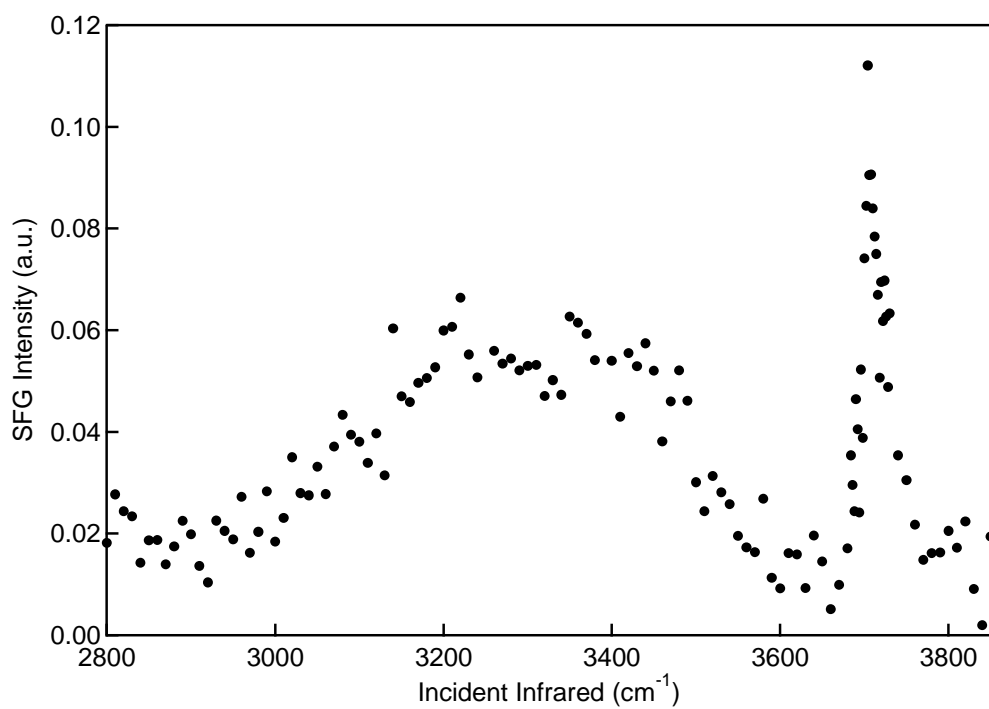
Figure 5.2 ssp VSFG normalized spectra of neat water.
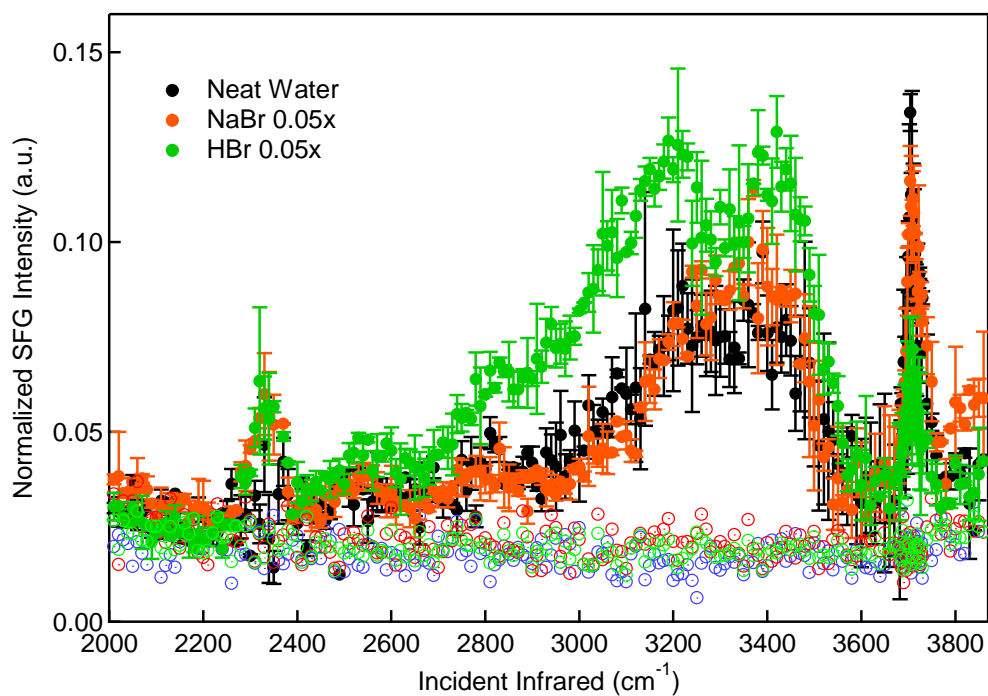
Figure 5.3 ssp-polarized SFG spectra of 0.05x HBr (green solid circles) and 0.050x NaBr (orange solid circles) compared to that of neat water (black solid circles) showing the proton continuum arising from the 0.05 mole fraction HBr solution. The open circles are the corresponding HBr (green open circles), NaBr (orange open circles), and neat water (black open circles) background spectra (the visible and infrared input pulses were temporally misaligned at the sample). The open circle data points show the actual background that contributes to the spectrum, confirming that the SFG intensities are real. Spectra obtained with the scanning SFG system.
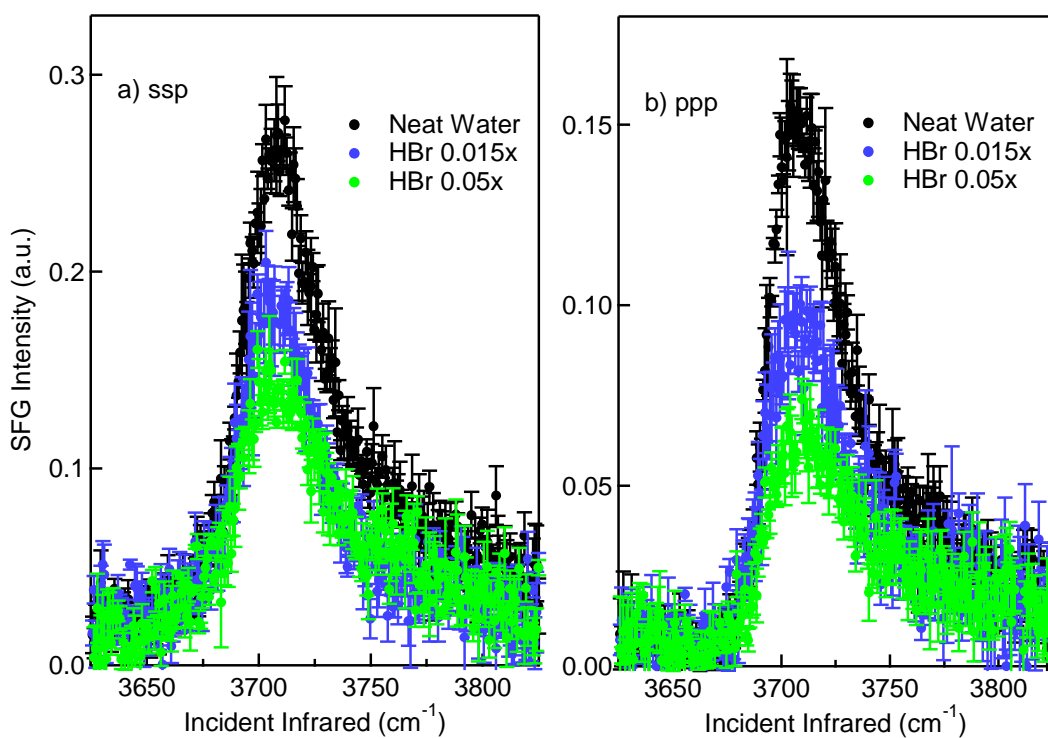
Figure 5.4 SFG spectra of 0.015x and 0.015x aqueous HBr under (a) ssp and (b) ppp polarization combinations. Error bars show the range (± standard deviation) of the intensities. Spectra acquired with the broad bandwidth SFG system.

Chapter 6

Environmental Implications and Future Work

The work presented in this thesis was motivated by an interest in understanding the surface structure of atmospheric aerosols. For this aim, atmospheric relevant model systems were investigated. A great number of organic compounds are emitted into the atmosphere from both biogenic and anthropogenic sources, therefore it is expected that a variety of organics exist within the surface region of atmospheric aerosols.

Mixed monolayers of fatty acid and alkyl halides were investigated as proxies of fat-coated marine aerosols. Fatty acids such as palmitic and stearic acid can coat the surface of marine aerosols affecting the surface properties of such aerosols. The presence of an insoluble fatty acid monolayer at the air-water interface affects the transport of volatile species through the interface. Long-chain alkyl halides can also coat marine aerosols if fatty acid molecules are present at the interface, thereby fatty acid films can transport alkyl halide molecules to the atmosphere which otherwise would be limited to remain on water surfaces. In addition to impeding the transport of gas-phase species, organic surface compounds will reduce the evaporation of water from the aerosol which in turn will enhance the aerosol lifetime. This can lead to the oxidizing of the film depending on the orientation and accessibility of the molecules in the film. It was found that alkyl halide

molecules have gauche defects in the mixed monolayers. Gauche defects have implications for reactivity (e.g. with OH radicals). At high surface pressures there is phase separation as the alkyl halide molecules are squeezed out which indicates that they will also separate in naturally occurring systems such as the monolayers found on fat-coated aerosols. The presence of organic compounds at the surface of atmospheric aerosols can reduce the growth rate of the aerosols since the film would impede the adsorption and uptake of volatile species.

The adsorption and uptake of atmospherically relevant gas-phase species (methyl chloride and methanol) to the air-water interface was also investigated. These gas-phase species can be adsorbed at the interface of atmospheric aerosol or like methyl chloride, they can be absorbed into the bulk. The presence of such species will modify the physical and chemical properties of atmospheric aerosols.

Additionally, the air-aqueous interface of aqueous HBr was investigated. The presences of H_3O^+ and $H_5O_2^{2+}$ at the air-water interface affect the physical characteristics and the chemistry of atmospheric aerosol surfaces, (i.e. hydrophobicity, particle growth, morphology, and acidity) which can lead to the adsorption and absorption of gas phase molecules. The adsorbed species can then participate in different reaction altering the atmospheric heterogeneous reactions.

In Appendix C an analysis of the BrHex decrease in IRRAS and SFG signal is performed. Future experiments are necessary to determine if BrHex molecules go the water subphase upon compression. To do this, enough water subphase should be taken and evaporated

(see Appendix C) to have an aliquot of > 2ppm of BrHex so it can be detected by the mass spectrometer (MS) or by Raman available in this lab.

Additional SFG experiments for the different alkyl halides at different ratios would help to understand the different behavior of each. These would include:

dPA-BrPent 3:1, 1:1, and 1:3

dPA-BrHex 3:1, and 1:3

dPA and ClHex 3:1, 1:1, and 1:3

Furthermore, the acquisition of SFG spectra in the C=O and OH vibrational regions would help to determine if the alkyl halide interacts with water molecules or with the carboxylic group of the fatty acid molecules.

As with the alkyl halides, mixed monolayer studies of alkanes are necessary to probe the minimum chain length for alkanes to incorporate into fatty acid monolayers. These experiments are important since a number of aliphatic hydrocarbons are emitted to the atmosphere.

Appendix A

Thermodynamic Analysis of Mixed Monolayer Isotherms

Mixed monolayers were studied to obtain information regarding their molecular packing and molecular orientation of their components. A number of parameters were used to characterize the degree of mixing and the stability of the monolayer, including MMA, collapse pressures, excess areas, and the excess Gibbs free energy of mixing as a function of RX mole fraction (x).

A.1 Mean Molecular Area

Analysis of MMA is used to characterize mixed films with respect to miscibility.[36,38,47,94] Thus, the surface pressure-area isotherms were analyzed in terms of mean molecular areas as a function of the alkyl halide mole fractions.

Mixed monolayers are analyzed in terms of area per molecule as a function of its alkyl halide composition at various surface pressures. The properties of a mixed monolayer will reflect those of the separate single component monolayers if they are immiscible. The area occupied by immiscible components which have no interactions between them in a mixed monolayer is the sum of the areas of the separate films. Assuming ideal miscibility or complete immiscibility in a two-component mixed monolayer at a given surface pressure, the MMA per molecule follows the additivity rule (eq A.1)[38,47,95]

$$A_{12} = x_1 A_1 + x_2 A_2 \qquad\qquad\qquad (A.1)$$

In eq A-1, x is the mole fraction, A the MMA, and the subscripts 1, 2, and 12 refer to the pure components 1 and 2 and their mixture, respectively. For this study, the subscript 1 refers to the fatty acid (dPA or dSA) and the subscript 2 to the alkyl halide (BrPent, BrHex or ClHex). Although this type of analysis for molecules that do not form monolayer by themselves is not found in the literature, A_2 is taken as zero in this dissertation. Taking A_2 as zero is somewhat controversial because BrHex molecules always occupy an area. In this analysis an A_2 of zero does not mean that alkyl halide molecules do not occupy an area on the water subphase. After spreading BrHex in chloroform on the water subphase, they occupy some space as it is observed in the BAM images (Figure 3.9). However, they form 3D aggregates which means that several molecules occupy the same area. Also, A_2 refers to the area per one molecule at a particular surface pressure in the monolayer. Since there is no monolayer, the area is considered to be zero.

Figure A.2 shows the experimental and ideal MMA as a function of alkyl halide mole fraction at different surface pressures for dPA and dSA mixed monolayers. Deviations from equation A.1 provide evidence for nonideal miscibility in a mixed monolayer. Negative deviations generally indicate attractive interactions between the components of the mixed film whereas positive deviations indicate the presence of repulsive interactions between the components of the film.[47,95-98] However, in these studies, negative deviations

are unlikely to occur because the area of pure RX (A_2 in equation A.1) is taken as zero. If RX molecules incorporate in the monolayer, regardless of the kind of interactions between the components of the mixture, the MMA will be larger than that of the pure fatty acid. In fact, experimental MMAs for all dPA and dSA systems (Figure A.2) show a positive deviation from equation A.1 at all surface pressures and mole fractions (experimental MMAs are greater than ideal MMAs). Since the alkyl halides do not form monolayers by themselves, the observed positive deviations suggest incorporation of alkyl halides into the fatty acid monolayer and nonideal miscibility.

From Figure A.2 we can see that the MMA decreases with x_2 consistent with the squeeze out of alkyl halides as the surface pressure increases, albeit at a rate that is not known. It is observed in Figure A.2 that at low surface pressure areas the largest difference between experimental and ideal MMA is for the BrHex mixed monolayers (C: dPA-BrHex and D: dSA-BrHex). Large MMA for the BrHex mixed monolayers suggest a more expanded conformation of the molecules compared to those of mixed monolayers with BrPent and ClHex (A, B, E and F). Nonetheless, it has been previously shown that as the alkyl chain length increases for an alkyl halide, the molecule orients more perpendicular to the surface.[22] MD simulations have shown that surface-adsorbed alkyl halides such as butyl halides are disordered with molecules predominantly aligned parallel to the surface whereas similar chain length alcohols orient perpendicular to the surface.[22] Thus, it is expected that BrHex occupies larger MMA than BrPent. As for the ClHex, chlorine atoms are smaller than bromine atoms and so it is expected that BrHex mixed monolayers molecules may occupy larger areas.

89

If the above analysis was done for dPA-alkane mixtures and using an A_2 of zero for the alkane molecules, no deviations from ideality (dotted lines in Figure A.2) would be estimated, indicating no incorporation of the alkane molecules in the fatty acid monolayer. For the dPA-alkane mixtures, we see that an A_2 of zero does not mean that the alkane molecules do not take space, it indicates they do not occupy space in the monolayer.

A.2 Excess Area

To further examine the miscibility of the mixed monolayers, the excess area was determined. The area of mixed monolayer can be compared to that of the unmixed, pure component monolayers by analyzing the excess area of mixing, which represents the difference in packing efficiency of the mixture components over the additive mixing values in which no interactions are present between the two components. Excess area is calculated by eq A.2.[95,99-102]

$$\Delta A_{exc} = A_{12} - x_1 A_1 - x_2 A_2 \tag{A.2}$$

In Figure A.3 plots of the excess area as a function of x_2 at different surface pressures are shown. If the components of the mixture are immiscible, the excess area is zero. Any deviation from this relationship indicates that the system is miscible. Condensing of the molecules leads to negative values of the excess area of mixing, whereas expansion leads to positive deviations. Both effects are due to geometric factors and hydrophobic

interactions.[47] However, in our case negative deviations are not expected since the x_2A_2 term is zero (recall that RX molecular areas are zero). Positive deviations are expected if component 2 (alkyl halide) is incorporated into component 1 (dPA or dSA). As shown in Figure A.3, both dPA and dSA mixed monolayers show positive ΔA_{exc} values at all mole ratios and surface pressures, which suggests incorporation of the corresponding alkyl halide molecules. It can also be observed from Figure A.3 that as the surface pressure increases, ΔA_{exc} decreases, indicating that the alkyl halide molecules are squeezed out of the fatty acid monolayer.

In a previous study, Peters and Rogers[37] showed that chlorooctadecane can form stable monolayers with SA up to 0.35x of alkyl halide. They found that for higher compositions molecules are squeezed out of the monolayer. In a different study, Ilharco et al[58] transferred cadmium heptadecanoate/chlorohexadecane and cadmium heptadecanoate/bromohexadecane to CaF_2 substrates for mole fractions of alkyl halides up to 0.3. In our investigation using dPA and dSA, the areas (MMA and ΔA_{exc}) suggest that at low surface pressures and low x_2 the components of the mixed monolayers are nonideally miscible. As the surface pressure increases the alkyl halide molecules are squeezed out. This analysis also suggests that alkyl halide molecules occupy smaller areas compared to the fatty acid molecules.

A.3 Excess Gibbs Free Energy of Mixing

Now that partial miscibility between the two components has been established, the excess Gibbs free energy of mixing (ΔG_{exc}) can be used as an indication of interactions

and stability of the mixed monolayer. Many authors[96-98,101-103] have determined the excess free energy of mixing from the surface pressure-area isotherms of the mixed monolayers following a method developed by Goodrich.[104] We have used eq A.3 according to Goodrich's method to calculate ΔG_{exc}.

$$\Delta G_{exc} = \int_{\pi^*}^{\pi} A_{12} d\pi - x_1 \int_{\pi^*}^{\pi} A_1 d\pi - x_2 \int_{\pi^*}^{\pi} A_2 d\pi \qquad\qquad (A\text{-}3)$$

The integrals equate the areas under the surface pressure-area isotherms. π^* is defined as the surface pressure where the monolayers are ideally miscible, which is assumed to be close to zero mN/m. In practice, π^* is set to the lowest measurable surface pressure. In this work, we set π^* to the surface pressure at the lift-off value of each isotherm, which was ~0.5 mN/m.

As with ΔA_{exc}, ideal mixing leads to an excess Gibbs free energy of zero, whereas negative deviations from ideality indicate the interaction between components is energetically favorable and the mixture is more stable. Positive deviations indicate some packing constraints suggesting the possibility of phase separation..[47,95,101,104]

Figure A.4 shows the calculated ΔG_{exc} at different surface pressures for all the systems. For all mixed monolayers, at low pressures positive values of ΔG_{exc} are observed and increase as the surface pressure is increased. We can also observe that ΔG_{exc} increases with alkyl halide concentration, which suggests the existence of repulsive interactions and separation phase. As the surface pressure increases, the intermolecular distances

become shorter, making molecular interactions between the mixed components less attractive which explains the increase of ΔG_{exc} with surface pressure. To conclude if there is separation phase the total free energy of mixing must be calculated according to eq A.4

$$\Delta G_{mix}^{tot} = \Delta G_{exc} + RT(x_1 \ln x_1 + x_2 \ln x_2) \tag{A.4}$$

Negative values of ΔG_{mix}^{tot} are calculated for all mixtures and compositions making phase separation unlikely.
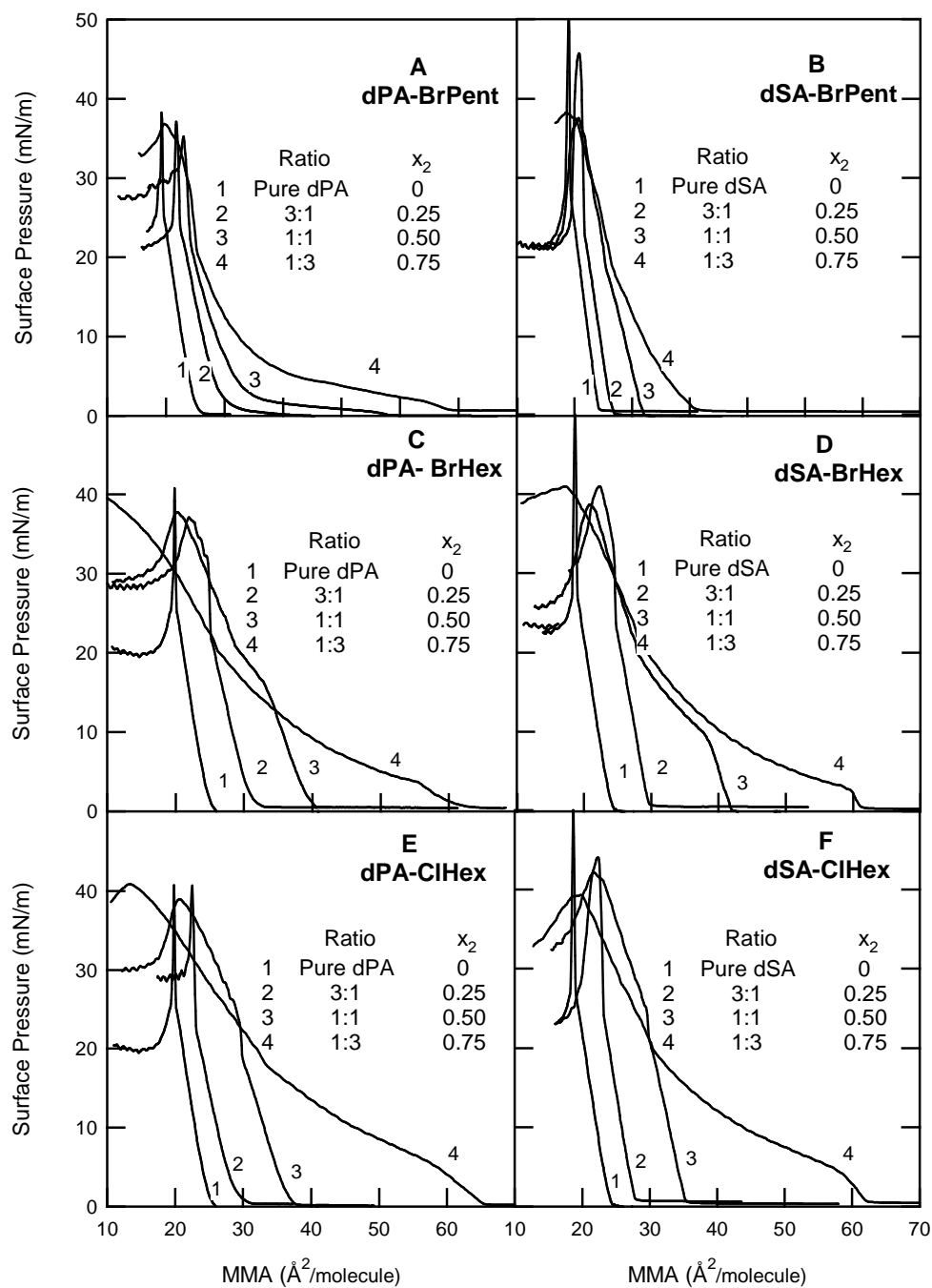
Figure A.1. Surface-pressure area per fatty acid molecule isotherms of mixed monolayers at different ratios of (a) dPA-BrPent, (b) dSA-BrPent, (c) dPA-BrHex, (d) dSA-BrHex, (e) dPA-ClHex, and (f) dSA-ClHex.

94
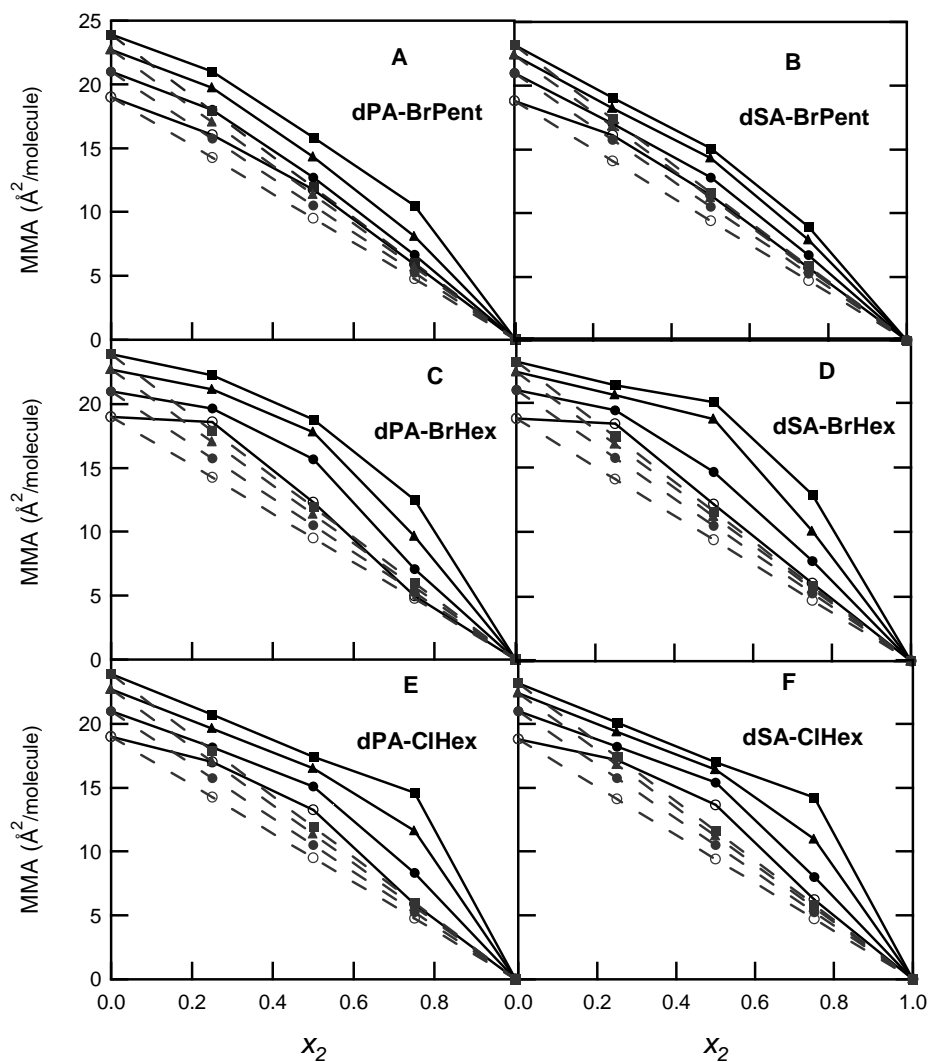
Figure A.2. Mean molecular area (MMA) of dPA and dSA mixed monolayers as a function of the alkyl halide molar fraction (x_2) at various surface pressures (■ 5 mN/m; ▲ 10 mN/m; ● 18 mN/m; ○ 30 mN/m). Experimental values ——. Ideal values - - - - -
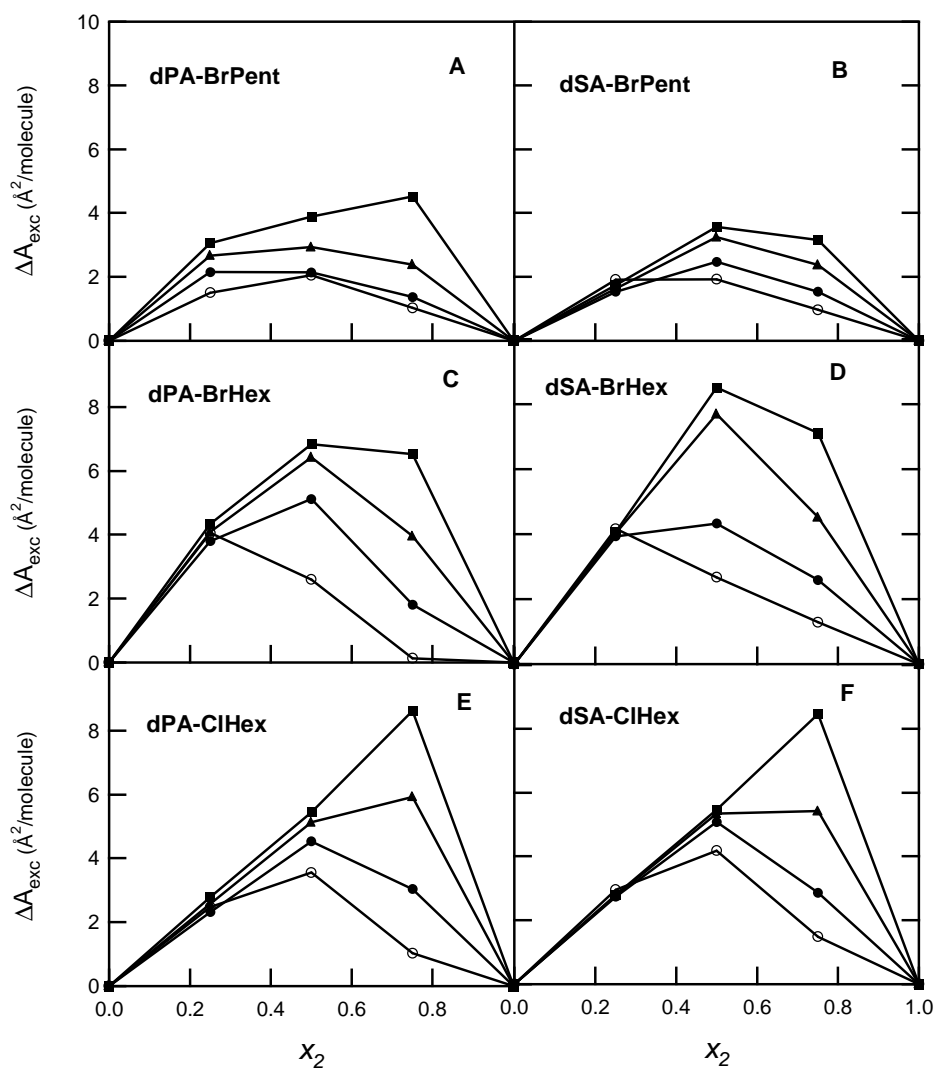
Figure A.3. Excess area (ΔA_{exc}) for mixed monolayers as a function of the alkyl halide molar fraction (x_2) at various surface pressures (■ 5 mN/m; ▲ 10 mN/m; ● 18 mN/m; ○ 30 mN/m).
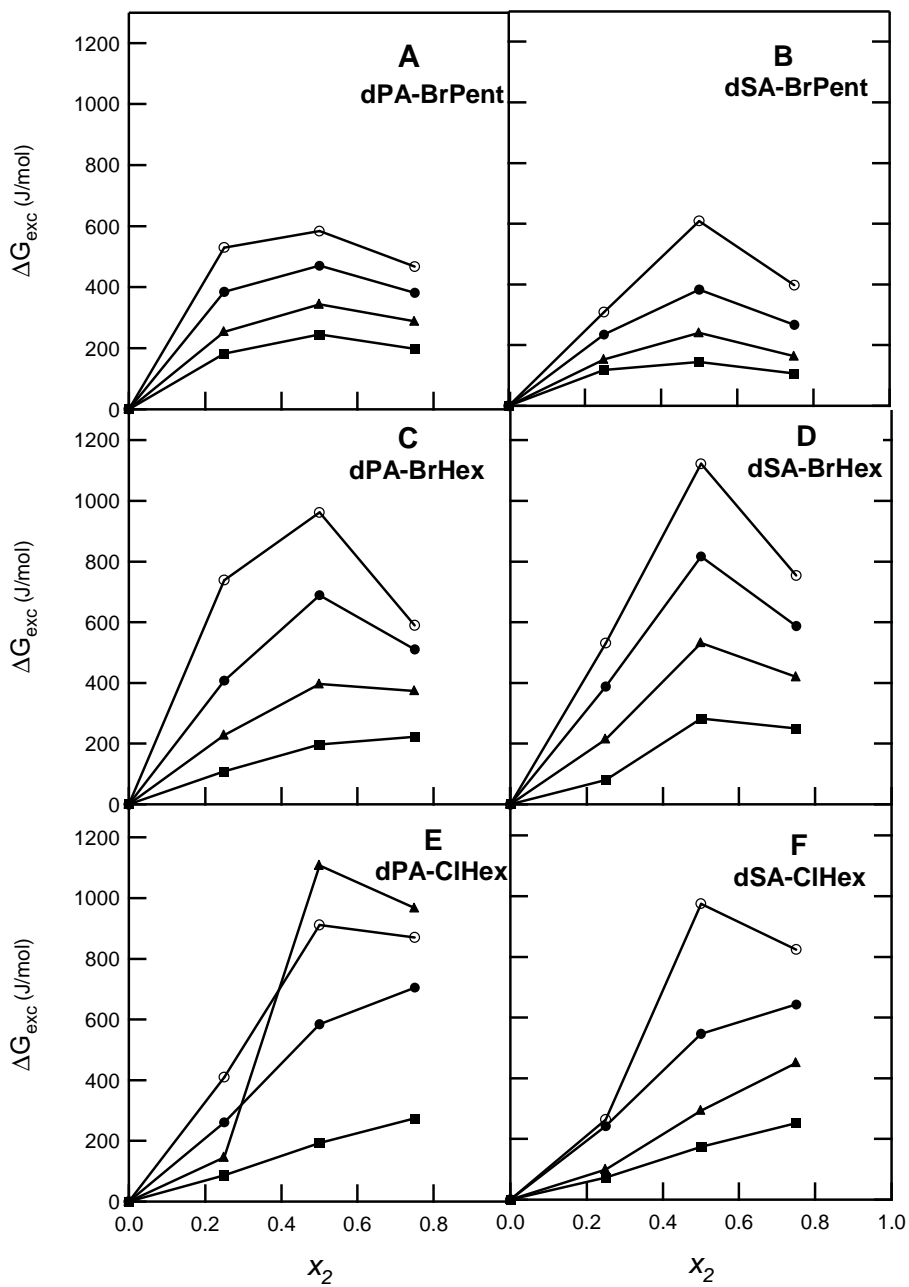
Figure A.4. Excess free energy (ΔG_{exc}) for mixed dPA and dSA monolayers as a function of the alkyl halide molar fraction (x_2) at various surface pressures (■ 5 mN/m; ▲ 10 mN/m; ● 18 mN/m; ○ 30 mN/m).

Appendix B

IRRAS Spectra of Mixed Monolayer with p polarization
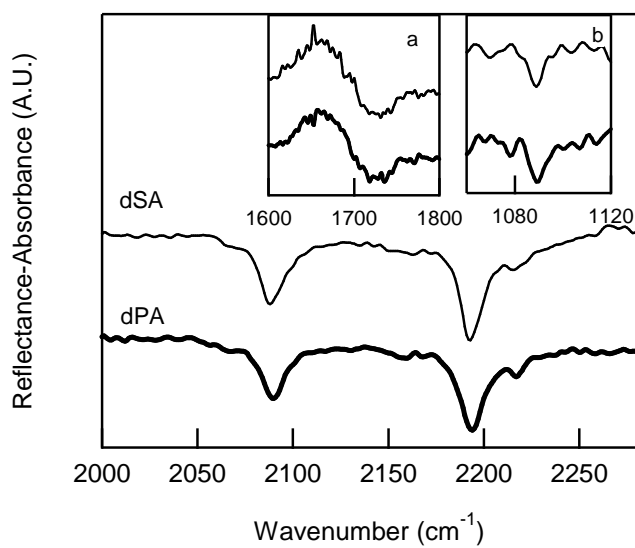
Figure B.1. IRRAS spectra of dPA and dSA on a water subphase at 25 mN/m respectively. Spectra were collected with p polarized light.
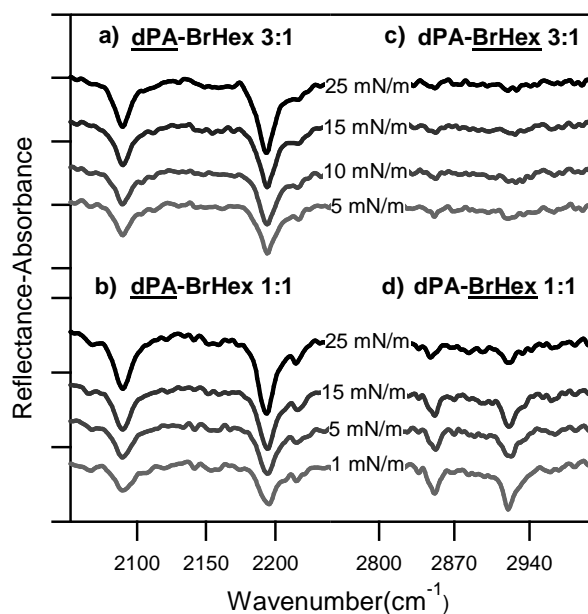
Figure B.2. IRRAS spectra of the dPA-BrHex mixture at 1, 5, 15, and 25 mN/m obtained with p polarized light. Panels a (dPA-BrHex 3:1) and b (dPA-BrHex 1:1) show the CD stretching region, which represents the dPA component in the monolayer. Panels c (dPA-BrHex 3:1) and d (dPA-BrHex 1:1) show the CH stretching region, which represents the BrHex component in the monolayer.
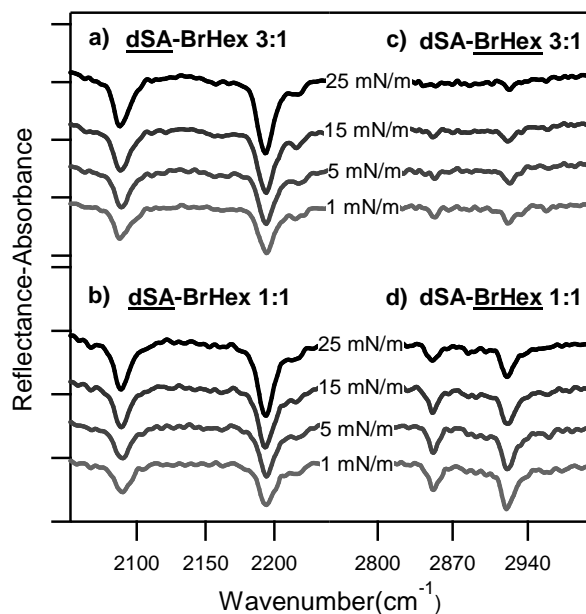
Figure B.3. IRRAS spectra of the dSA-BrHex mixture at 1, 5, 15, and 25 mN/m obtained with p polarized light. Panels a (dSA-BrHex 3:1) and b (dSA-BrHex 1:1) show the CD stretching region, which represents the dPA component in the monolayer. Panels c (dSA-BrHex 3:1) and d (dSA-BrHex 1:1) show the CH stretching region, which represents the BrHex component in the monolayer.

Appendix C

Analysis of the BrHex Decrease in IRRAS and SFG Signal

The SFG and IRRAS results in Chapter 3 revealed that alkyl halide molecules incorporate into the dPA and dSA monolayer, and that they are not retained as surface pressure increases. This was concluded by the decrease in the IRRAS and SFG intensity, which indicates a decrease in the number of molecules being probed. One question arises from this, where do BrHex molecules go? To answer this question, all possibilities are analyzed.

BrHex molecules in the mixed monolayer can go to:

1. gas phase

2. top of the monolayer

3. remain in the dPA monolayer

4. walls of the trough

5. water subphase

Evaporation of BrHex to the gas phase is unlikely since its vapor pressure < 1 torr at 20°C. This is approximately 20 times less volatile than water at this temperature. To corroborate the low volatility of BrHex, an evaporation test was performed. 1 ml of pure BrHex was placed on a Petri dish and weight in an analytical balance (accuracy to 0.1

mg) over a period of 48 hrs. No evaporation loss was observed. Therefore, evaporation of BrHex is ruled out.

If BrHex molecules remain in the dPA monolayer, it would be expected to obtain SFG signal. However, it is observed in Figure 3.2 c the absence of CH signal at 25 mN/m which indicates that BrHex is not in the mixed monolayer. On the other hand, IRRAS signal of CH peaks is still observed at high surface pressures. IRRAS as opposed to SFG does not require a lack of inversion symmetry and therefore when we see IRRAS signal from the CH peaks we can only conclude that BrHex molecules are being probed either in the dPA monolayer, on top of the monolayer, or both. Since SFG suggests that BrHex molecules are not in the dPA monolayer, one can conclude that the BrHex molecules probed by IRRAS should be on top of the monolayer after also considering dispersion forces between the tail groups of both molecules.

Another possibility for the BrHex molecules is to move to the walls of the trough which are hydrophobic, although the barriers are made of hydrophilic Delrin. However this is unlikely since BAM images of pure BrHex showed aggregates of it on the water subphase, distant from the trough walls.

In a different experiment, pure BrHex and water were mixed in a Petri dish. After agitation, the BrHex emulsified in the water. This suggested that BrHex could emulsify in the water subphase under compression. To determine if BrHex molecules go to the water subphase, approximately 60 ml of water subphase were taken from the trough after compression of a dPA-BrHex 1:1 monolayer, making sure the monolayer was not disturbed. Then, this aliquot was evaporated at low temperature on a hot plate until the

103

volume was ~ 5 ml (a 10 times decrease in volume). This was then analyzed by Raman spectroscopy. The Raman spectrometer employed in this experiment uses a 532 nm continuous wave laser (Process Instruments; model PI-ECL-785-300-SH) as an excitation source. The laser beam (0.2 mW) is delivered to the sample by the same fiber optic probe (InPhotonics) used to collect the scattered light. The scattered light was dispersed by a 600 g/mm grating blazed at 1 μm in a 500 mm monochromator (Acton Research, SpectraPro 500i; 50 μm slit width) and detected using a liquid nitrogen cooled CCD (Roper Scientific, LN 400EB, back-illuminated, deep depletion, 1340×400 pixel array). If BrHex goes to the water subphase, a C-Br peak would be observed at ~ 600 cm^{-1}. The Raman spectrum did not show the C-Br peak, this can be due to the absence of BrHex or the detection limits of the instrument. Typical detection limits in Raman spectroscopy are in the parts per million (ppm) or parts per thousand (ppth) for sampling solvated organics in aqueous media and is discussed below.

Considering that 60 microliter (μl) of a 2 millimolar (mM) dPA-BrHex (1:1) solution in chloroform are spread on a 100 ml water subphase and assuming that all of the BrHex emulsifies in the water subphase, the concentration of BrHex, if fully emulsified in the subphase, would be 0.6 μM (183 ppb by weight; moles BrHex to volume of water assuming 1 ml= 1 g). This concentration is below the detection limit of the Raman, which as stated above is in the ppm or ppth range, which may explain the absence of C-Br signal.

$$\frac{2.0\,mmolesBrHex}{1LBrHex \cdot solution} \times 3.0 \times 10^{-2}\,mlBrHex \cdot solution \times \frac{1}{1 \times 10^{2}\,mlH_{2}O} \times \frac{3.05 \times 10^{2}\,gBrHex}{1moleBrHex} \times$$

$$\frac{1mlH_{2}O}{1gH_{2}O} = \frac{1.83 \times 10^{-2}\,gBrHex}{1 \times 10^{5}\,gH_{2}O} = 183\,ppb$$

To further determine if BrHex is in the water subphase, the water subphase after evaporation was analyzed by mass spectrometry. A Bruker microTOF mass spectrometer (MS) with electrospray ionization, time-of-flight (TOF) mass analyzer and Faraday cup detector was used. The manufacturer specifies a detection limit for this MS of < 2 ppm. The MS spectrum did not show any peak from the BrHex, this can be due to the detection limits of the instrument.

This analysis suggests that upon compression some BrHex molecules remain on top of the dPA monolayer (suggested by the IRRAS spectra) and others emulsify in the water subphase. However, future studies should readdress this by additionally concentrating the subphase and reanalyzing.

References

(1)   Finlayson-Pitts, B. J. Reactions at surfaces in the atmosphere: integration of experiments and theory as necessary (but not necessarily sufficient) for predicting the physical chemistry of aerosols. *Phys. Chem. Chem. Phys.* **2009**, *11*, 7760-7779.

(2)   Prather, K. A.; Hatch, C. D.; Grassian, V. H. Analysis of atmospheric aerosols. *Annu. Rev. Anal. Chem.* **2008**, *1*, 485-514.

(3)   Patel, M. M.; Miller, R. L. Air pollution and childhood asthma: recent advances and future directions. *Curr. Opin. Pediatr.* **2009**, *21*, 235-241.

(4)   Pope III, C. A.; Dockery, D. W. Health effects of fine particulate air pollution: lines that connect. *J. Air & Waste Manage. Assoc.* **2006**, *56*, 709–742.

(5)   IPCC "Climate change the physical science basis," 2007.

(6)   Rosenfeld, D. Aerosols, clouds, and climate. *Science* **2006**, *312*, 1323-1324.

(7)   Molina, M. J.; Tso, T.-L.; Molina, L. T.; Wang, F. C.-Y. Antarctic stratospheric chemistry of chlorine nitrate, hydrogen chloride, and ice: release of active chlorine. *Science* **1987**, *238*, 1253-1257.

(8)   Finlayson-Pitts, B. J.; Pitts, J. N. J. *Chemistry of the upper and lower atmosphere: theory, experiments, and applications*; Academic Press: San Diego, 2000.

(9)   Aiken, A. C.; Salcedo, D.; Cubison, M. J.; Huffman, J. A.; DeCarlo, P. F.; Ulbrich, I. M.; Docherty, K. S.; Sueper, D.; Kimmel, J. R.; Worsnop, D. R.; Trimborn, A.; Northway, M.; Stone, E. A.; Schauer, J. J.; Volkamer, R. M.; Fortner, E.; de Foy, B.; Wang, J.; Laskin, A.; Shutthanandan, V.; Zheng, J.; Zhang, R.; Gaffney, J.; Marley, N. A.; Paredes-Miranda, G.; Arnott, W. P.; Molina, L.; Sosa, G.; Jimenez, J. L. Mexico City aerosol analysis during MILAGRO using high resolution aerosol mass spectrometry at the urban supersite (T0) – Part 1: Fine particle composition and organic source apportionment. *Atmos. Chem. Phys.* **2009**, *9*, 6633–6653.

(10)   Jimenez, J. L.; Jayne, J. T.; Shi, Q.; Kolb, C. E.; Worsnop, D. R.; Yourshaw, I.; Seinfeld, J. H.; Flagan, R. C.; Zhang, X.; Smith, K. A.; Morris, J. W.; Davidovits, P. Ambient aerosol sampling using the Aerodyne Aerosol Mass Spectrometer. *J. Geophys. Res.* **2003**, *108*, 8425 (13-1- 13-13).

(11)   Sun, J.; Zhang, Q.; Canagaratna, M. R.; Zhang, Y.; Ng, N. L.; Sun, Y.; Jayne, J. T.; Zhang, X.; Zhang, X.; Worsnop, D. R. Highly time- and size-resolved characterization of submicron aerosol particles in Beijing using an Aerodyne Aerosol Mass Spectrometer. *Atmos. Env.* **2010**, *44*, 131-140.

(12)   Tsimpidi, A. P.; Karydis, V. A.; Zavala, M.; Lei, W.; Molina, L.; Ulbrich, I. M.; Jimenez, J. L.; Pandis, S. N. Evaluation of the volatility basis-set approach for the simulation of organic aerosol formation in the Mexico City metropolitan area. *Atmos. Chem. Phys.* **2010**, *10*, 525-546.

(13)   Knipping, E. M.; Lakin, M. J.; Foster, K. L.; Jungwirth, P.; Tobias, D. J.; Gerber, R. B.; Dabdub, D.; Finlayson-Pitts, B. J. Experiments and simulations of ion-enhanced interfacial chemistry on aqueous NaCl aerosols. *Science* **2000**, *288*, 301-306.

(14)   Hu, J. H.; Davidovits, P.; Worsnop, D. R.; Zahniser, M. S.; Kolb, C. E. Reactiveuptake of Cl2(g) and Br2(g) by aqueous surfaces as a function of Br- and I- ion concentration: Theeffect of chemical reaction at the interface. *J. Phys. Chem.* **1995**, *99*, 8768-8776.

(15)   Jayne, J. T.; Davidovits, P.; Worsnop, D. R.; Zahniser, M. S.; Kolb, C. E. Uptake of SO2(g) by aqueous surfaces as a function of pH: The effect of chemical reaction at the Iinterface. *J. Phys. Chem.* **1990**, *94*, 6041-6048.

(16)   Donaldson, D. J.; Guest, J. A.; Goh, M. C. Evidence for adsorbed SO2 at the aqueous-air Interface. *J. Phys. Chem.* **1995**, *99*, 9313-9315.

(17)   Duce, R. A.; Quinn, J. G.; Olney, C. E.; Piotrowicz, S. R.; Ray, B. J.; Wade, T. L. Enrichment of Heavy Metals and Organic Compounds in the Surface Microlayer of Narragansett Bay, Rhod Island. *Science* **1972**, *176*, 161-163.

(18)   Gagosian, R. B.; Peltzeer, E. T.; Zafiriour, O. C. Atmospheric transport of continentally derived lipids to the tropical North Pacific. *Nature* **1981**, *291*, 312-314.

(19)   Gill, P. S.; Graedel, T. E.; Weschler, C. J. *Rev. Geophys. Space Phys.* **1983**, *21*, 903.

(20)   Tervahattu, H.; Juhanoja, J.; Kupiainen, K. *J. Geophys. Res.* **2002**, *D16*, ACH18/1.

(21)   Tervahattu, H.; Juhanoja, J.; Vaida, V.; Tuck, A. F.; Niemi, J. V.; Kupiainen, K.; Kulmala, M.; H. Vehkamäki, H. Fatty acids on continental sulfate aerosol particles. *J. Geophys. Res.* **2005**, *110*, D06207.

(22)   Harper, K.; Minofar, B.; Sierra-Hernandez, M. R.; Casillas-Ituarte, N. N.; Roeselova, M.; Allen, H. C. Surface residence and uptake of methyl chloride and methyl alcohol at the air/water interface studied by vibrational sum frequency spectroscopy and molecular dynamics. *J. Phys. Chem. A* **2009**, *113*, 2015-2024.

(23)   Gericke, A.; Michailov, A. V.; Hühnerfuss, H. Polarized external infrared reflection-absorption spectrometry at the air/water interface: comparison of experimental and theoretical results for different angles of incidence. *Vib. Spec.* **1993**, *4*, 335-348.

(24)   Mendelsohn, R.; Brauner, J. W.; Gericke, A. External infrared reflection absorption spectrometry of monolayer films at the air-water interface. *Annu. Rev. Phys. Chem.* **1995**, *46*, 305-334.

(25)   Yamamoto, K.; Ishida, H. Optical theory applied to infrared spectroscopy. *Vib. Spec.* **1994**, *8*, 1-36.

(26)   Kuzmin, V. L.; Michailov, A. V. *Opt. Spectrosc.* **1981**, *51*, 383-385.

(27)   Fina, L. J.; Tung, Y.-S. Molecular orientation of monolayers on liquid substrates: optical model and FT-IT methods. *Appl. Spectrosc.* **1991**, *45*, 986-992.

(28)   Hirose, C.; Akamatsu, N.; Domen, K. J. Formulas for the analysis of surface sum-frequency generation spectrum by CH stretching modes of methyl and methylene groups. *J. Chem. Phys.* **1992**, *96*, 997-1004.

(29)   Lambert, A. G.; Davies, P. B.; Neivandt, D. J. Implementing the theory of sum frequency generation vibrational spectroscopy: a tutorial review. *Appl. Spectrosc. Rev.* **2005**, *40*, 103-145.

(30)   Shen, Y. R. *The principles of nonlinear optics*; Wiley: New York, 1984.

(31)   Henon, S.; Meunier, J. Microscope at the Brewster angle: direct observation of first-order phase transitions in monolayers. *Rev. Sci. Instrum.* **1991**, *62*, 936-939.

(32)   Honig, D.; Mobius, D. Direct visualization of monolayers at the air-water interface by Brewster angle microscopy. *J. Phys. Chem.* **1991**, *95*, 4590-4592.

(33)   Hommel, E. L.; Ma, G.; Allen, H. C. *Anal. Lett.* **2001**, *17*, 1325.

(34)   Ma, G.; Allen, H. C. *J. Phys. Chem. B* **2003**, *107*, 6343.

(35)   Baskar, G.; Shanmugharaj, A. M.; Venkatesh, S.; Mandal, A. B. Incorporation of bromo-octadecane into long-chain ester monolayers at the air/water interface. *Journal of the American Oil Chemists* **2001**, *78*, 503-507.

(36)   Gonçalves da Silva, A. M.; Guerreiro, J. C.; Rodrigues, N. G.; Rodrigues, T. O. Mixed monolayers of heptadecanoic acid with chlorohexadecane and bromohexadecane. Effects of temperature and of metal ions in the subphase. *Langmuir* **1996**, *12*, 4442-4448.

(37)   Peters, A.; Rogers, K. The production of stable monolayers from nonamphiphilic 1-chlorooctadecane. *J. Colloid Interface Sci.* **1993**, *157*, 511-512.

(38)   Gaines, G. L. *Insoluble monolayers at liquid-gas interfaces*; Interscience Publishers: New York, 1966.

(39)   Ma, G.; Allen, H. C. Condensing effect of palmitic acid on DPPC in mixed Langmuir monolayers. *Langmuir* **2007**, *23*, 589 - 597.

(40)   Tang, C.; Allen, H. C. Ionic binding of Na+ vs K+ to the carboxylic acid head group pf palmitic acid monolayers studied by VSFG. *J. Phys. Chem. A* **2009**, *113*, 7383-7393.

(41)   Voss, L. F.; Hadad, C. M.; Allen, H. C. Competition between atmospherically relevant fatty acid monolayers at the air/water interface. *J. Phys. Chem. B* **2006**, *110*, 19487-19490.

(42)   Adam, N. K. *The physics and chemistry of surfaces*, 3rd ed.; Oxford University Press: London, 1941.

(43)   Guyot-Sionnest, P.; Hunt, J. H.; Shen, Y. R. Sum-frequency vibrational spectroscopy of a Langmuir film:study of molecular orientation of a two-dimensional system. *Phys. Rev. E* **1987**, *59*, 1597-1600.

(44)   Gericke, A.; Hühnerfuss, H. In situ investigation of saturated long-chain fatty acids at the air/water Interface by external infrared reflection-absorption spectrometry. *J. Phys. Chem.* **1993**, *97*, 12899-12908.

(45)   Adamson, A. W.; Gast, A. P. *Physical chemistry of surfaces*, 6th ed.; Wiley: New York, 1997.

(46)   Kaganer, V. M.; Möhwald, H.; Dutta, P. Structure and phase transitions in Langmuir monolayers. *Rev. Mod. Phys.* **1999**, *71*, 779-819.

(47)   Dynarowicz-Latka, P.; Kita, K. Molecular interaction in mixed monolayers at the air-water interface. *Adv. Colloid. Interface Sci.* **1999**, *79*, 1-17.

(48) Thornton, J. A.; Kercher, J. P.; Riedel, T. P.; Wagner, N. L.; Cozic, J.; Holloway, J. S.; Dube', W. P.; Wolfe, G. M.; Quinn, P. K.; Middlebrook, A. M.; Alexander, B.; Steven S. Brown, S. S. A large atomic chlorine source inferred from mid-continental reactive nitrogen chemistry. *Nature* **2010**, *464*, 271-274.

(49) Graedel, T. E.; Keen, W. C. Tropospheric budget of reactive chlorine. *Global Biogeochem. Cycles* **1995**, *9*, 47-77.

(50) Keene, W. C.; Khalil, M. A. K.; Erickson, D. J., III; McCulloch, A.; Graedel, T. E.; Lobert, J. M.; Aucott, M. L.; Gong, S. L.; Harper, D. B.; Kleiman, G.; Midgley, P.; Moore, R. M.; Seuzaret, C.; Sturges, W. T.; Benkovitz, C. M.; Koropalov, V.; Barrie, L. A.; Li, Y. F. Composite global emissions of reactive chlorine from anthropogenic and natural sources: Reactive Chlorine Emissions Inventory. *Journal of Geophysical Research, [Atmospheres]* **1999**, *104*, 8429-8440.

(51) Lovelock, J. E.; Maggs, R. J.; Wade, R. J. Halogenated hydrcarbons in and over the Atlantic. *Nature* **1973**, *241*, 194-196.

(52) Carpenter, L. J.; Sturges, W. T.; Penkett, S. A.; Liss, P. S.; Alicke, B.; Hebestreit, K.; Platt, U. Short-lived alkyl iodides and bromides at Mace Head, IIreland: links to biogenic sources and halogen oxide production. *J. Geophys. Res.* **1999**, *104*, 1679-1689.

(53) Butler, J. H. Atmospheric chemistry: better budgets for methyl halides? *Nature (London)* **2000**, *403*, 260-261.

(54) Ashizuka, Y.; Nakagawa, R.; Tobiishi, K.; Hori, T.; Iida, T. Determination of polybrominated diphenyl ethers and polybrominated dibenzo-p-dioxins/dibenzofurans in marine products. *J. Ag. Food. Chem.* **2005**, *53*, 3807-3813.

(55) Faulkner, D. J. Marine natural products. *Nat. Prod. Rep.* **2001**, *18*, 1-49.

(56) Kotterman, M.; van der Veen, I.; van Hesselingen, J.; Leonards, P.; Osinga, R.; de Boer, J. Preliminary study on the occurrence of brominated organic compounds in Dutch marine organisms. *Biom. Eng.* **2003**, *20*, 425-426.

(57) Nutting, G. C.; Harkins, W. D. Pressure-area relations of fatty acid and alcohol monolayers. *J. Am. Chem. Soc.* **1939**, *61*, 1182.

(58) Ilharco, L. M.; Garcia, A. R.; Fidalgo, A. M.; Barros, R.; Vale, A. F.; Lopes da Silva, J.; Gonçalves da Silva, A. M. A transmission FTIR spectroscopic study on mixed Langmuir-Blodgett Films of cadmium heptadecanoate-chloro/bromohexadecane. *Langmuir* **1995**, *11*, 2745-2750.

(59) Lee, K. Y. C. Collapse mechanisms of Langmuir monolayers. *Annu. Rev. Phys. Chem.* **2008**, *59*, 771-791.

(60) Yang, C. S.-C.; Richter, L. J.; Stephenson, J. C.; Briggman, K. A. In situ, vibrationally resonant sum frequency spectroscopy study of the self-assembly of dioctadecyl disulfide on gold. *Langmuir* **2002**, *18*, 7549-7556.

(61) Eisenthal, K. B. Equilibrium and dynamic processes at interfaces by second harmonic and sum frequency generation. *Annu. Rev. Phys. Chem.* **1992**, *43*, 627-661.

(62) Zhang, D.; Gutow, J.; Eisenthal, K. B. Vibrational spectra, orientations, and phase transitions in long-chain amphiphiles at the air/water interface: probing the

head and tail groups by sum frequency generation. *J. Phys. Chem.* **1994**, *98*, 13729-13734.

(63)   Wang, C.-y.; Groenzin, H.; Shultz, M. J. Surface characterization of nanoscale TiO_2 film by sum frequency generation using methanol as a molecular probe. *J. Phys. Chem. B* **2004**, *108*, 265-272.

(64)   Conboy, J. C.; Messmer, M. C.; Richmond, G. L. Dependence of alkyl chain conformation of simple ionic surfactants on head group functionality as studied by vibrational sum-frequency spectroscopy. *J. Phys. Chem. B* **1997**, *101*, 6724-6733.

(65)   Weidemann, G.; Brezesinski, G.; Vollhardt, D.; Bringezu, F.; de Meijere, K.; Mohwald, H. Comparing molecular packing and textures of Langmuir monolayers of fatty acids and their methyl and ethyl esters. *J. Phys. Chem. B* **1998**, *102*, 148-153.

(66)   Lee, K. Y. C.; Gopal, A.; von Nahmen, A.; Zasadzinski, J. A.; Majewski, J.; Smith, G. S.; Howes, P. B.; Kjaer, K. Influence of palmitic acid and hexadecanol on the phase transition temperature and molecular packing of dipalmitoylphosphatidyl-choline monolayers at the air–water interface. *J. Chem. Phys.* **2002**, *116*, 774.

(67)   Wang, H.-F.; Gan, W.; Lu, R.; Rao, Y.; Wu, B.-H. Quantitative spectral and orientational analysis in surface sum frequency generation vibrational spectroscopy (SFG-VS). *Int. Rev. Phys. Chem.* **2005**, *24*, 191-256.

(68)   Van Loon, L. L.; Minor, R. N.; Allen, H. C. structure of butanol and hexanol at aqueous, ammonium bisulfate, and sulfuric acid solution surfaces investigated by vibrational sum frequency generation spectroscopy. *J. Phys. Chem. A* **2007**, *111*, 7338-7346.

(69)   Xu, M.; Liu, D.; Allen, H. C. Ethylenediamine at air/liquid and air/silica interfaces: protonation versus hydrogen bonding investigated by sum frequency generation spectroscopy. *Environ. Sci. Technol.* **2006**, *40*, 1566-1572.

(70)   Brauner, J. W.; Flach, C. R.; Xu, Z.; Bi, X.; Lewis, R. N. A. H.; McElhaney, R. N.; Gericke, A.; Mendelsohn, R. Quantitative functional group orientatin in langmuir films by infrared relfection-absorption spectroscopy: C=O groups in behenic acid methyl ester and sn2-C-DSPC. *J. Phys. Chem. B* **2003**, *107*, 7202-7211.

(71)   Snyder, R. G.; Liang, G. L.; Strauss, H. L.; Mendelsohn, R. IR spectroscopic study of the structure and phase behavior of long-chain diacylphosphatidylcholines in the gel state. *Biophys. J.* **1996**, *71*, 3186-3198.

(72)   Sun, W.-J.; Tristram-Nagle, S.; Suter, R. M.; Nagle, J. F. Anomalous phase behavior of long chain saturated lecithin bilayers. *Biochim. Biophys. Acta* **1996**, *1279*, 17-24.

(73)   Qi, S.; Roser, S. J.; Deutsch, D.; Barker, S. A.; Craig, D. Q. M. A laser imaging and neutron reflection investigation into the monolayer behaviour of fatty acids used for taste masking microspheres. *J. Pharm. Sci.* **2008**, *97*, 1864-1877.

(74)   Flach, C. R.; Mendelsohn, R.; Rerek, M. E.; Moore, D. J. Biophysical studies of model stratum corneum lipid monolayers by infrared reflection-absorption spectroscopy and Brewster angle microscopy. *J. Phys. Chem. B* **2000**, *104*, 2159-2165.

(75)   Lee, Y. T.; Yang, Y.-C.; Shen, Y.-J. Monolayer characteristics of mixed octadecylamine and stearic at the air-water interface. *J. Phys. Chem. B* **2005**, *109*, 4662-4667.

110

(76)   Harper, K. Interfacial vibration chemistry of I. Mixed surfactant systems, II. Alkyl halide uptake and atmospheric Implications. MSc, The Ohio State University, 2007.

(77)   Casillas-Ituarte, N. N. Spectroscopic studies of atmospheric relevant air-aqueous and air-sililca interfaces. Doctorate, The Ohio State University, 2010.

(78)   Rothman, L. S. J., D.; Barbe, A. Chris Benner, D.; Birk, M.;; Brown, M. R. C., L.R.; Chackerian Jr, C.; Chance, K.; Coudert, L.H.;; Dana, V. D., V. M.; Flaud, J.-M.; Gamache, R. R.; Goldman, A.;; Hartmann, J.-M. J., K.W.; Maki, A.G.; Mandin, J.-Y.; Massie, S.T.;; Orphal, J. P., A.; Rinsland, C.P.; Smith, M.A.H.; Tennyson, J.;Tolchenov, R. N.; Toth, R.A.; Vander Auwera, J.; Varanasiq, P.; Wagner, G. The HITRAN 2004 molecular spectroscopic database. *Journal of Quantitative Spectroscopy & Radiative Transfer* **2005**, *96*, 139-204.

(79)   Liu, D.; Ma, G.; Levering, L. M.; Allen, H. C. Vibrational spectroscopy of equeous sodium halide solutions and air-;iquid interfaces: observation of increased interfacial depth. *J. Phys. Chem. B* **2004**, *108*, 2252-2260.

(80)   Levering, L. M. A vibrational spectroscopic study of aqueous hydrogen halide solutions: application to atmospheric aerosol chemistry. MSc, The Ohio State University, 2005.

(81)   Allen, H. C.; Casillas-Ituarte, N. N.; Sierra-Hernandez, M. R.; Chen, X.; Tang, C. Y. Shedding light on water structure at air-aqueous interfaces: ions, lipids, and hydration. *Phys. Chem. Chem. Phys.* **2009**, *11*, 5538-5549.

(82)   Levering, L. M.; Sierra-Hernandez, M. R.; Allen, H. C. Observation of hydronium ions at the air-aqueous acid interface: vibrational spectroscopic studies of aqueous HCl, HBr, and HI. *J. Phys. Chem. C* **2007**, *111*, 8814-8826.

(83)   Smith, J. D.; Cappa, C. D.; Wilson, K. R.; Cohen, R. C.; Geissler, P. L.; Saykally, R. J. Unified description of temperature-dependent hydrogen-bond rearrangements in liquid water. *Proc. Natl. Acad. Sci.* **2005**, *102*, 14171-14174.

(84)   Mucha, M.; Frigato, T.; Levering, L. M.; Allen, H. C.; Tobias, D. J.; Dang, L. X.; Jungwirth, P. A unified molecular picture of the surfaces of aqueous acid, base, and salt solutions. *J. Phys. Chem. B* **2005**.

(85)   Petersen, M. K.; Saykally, R. J. Evidence for an enhanced hydronium concentration at the liquid water surface. *J. Phys. Chem. B* **2005**, *109*, 7976-7980.

(86)   Tarbuck, T. L.; Ota, S. T.; Richmond, G. L. Spectroscopic studies of solvated hydrogen and hydroxide ion at aqueous surfaces. *J. Am. Chem. Soc.* **2006**, *128*, 14519-14527.

(87)   Petersen, M. K.; Iyengar, S. S.; Day, T. J. F.; Voth, G. A. The hydrated proton at the water liquid/vapor interface. *J. Phys. Chem. B* **2004**, *108*, 14804-14806.

(88)   Yeh, L. I.; Okumura, M.; Myers, J. D.; Price, J. M.; Lee, Y. T. Vibrational spectroscopy of the hydrated hydronium cluster ions $H3O+\times(H2O)n$ (n = 1, 2, 3). *J. Chem. Phys.* **1989**, *91*, 7319-7330.

(89)   Graham, J. D.; Roberts, J. T. Formation of $HCl\times6H_2O$ from ice and HCl under ultrahigh vacuum. *Chemom. Intell. Lab. Syst.* **1997**, *37*, 139-148.

(90)   Kim, J.; Schmitt, U. W.; Gruetzmacher, J. A.; Voth, G. A.; Scherer, N. E. The vibrational spectrum of the hydrated proton: Comparison of experiment, simulation, and normal mode analysis. *J. Chem. Phys.* **2002**, *116*, 737-746.

(91)   Gan, W.; Wu, D.; Zhang, Z.; Guo, Y.; Wang, H. F. Orientation and motion of water molecules at air/water interface. *Chinese Journal of Chemical Physics* **2006**, *19*, 20-24.

(92)   Wei, X.; Shen, Y. R. Motional effect in surface sum-frequency vibrational spectroscopy. *Physical Review Letters* **2001**, *86*, 4799-4802.

(93)   Gan, W.; Wu, D.; Zhang, Z.; Feng, R. R.; Wang, H. F. Polarization and experimental configuration analyses of sum frequency generation vibrational spectra, structure, and orientational motion of the air/water interface. *Journal of Chemical Physics* **2006**, *124*, 114705.

(94)   Cordroch, W.; Möbius, D. Incorporation of non-amphiphilic compounds into host monolayers. *Thin Solid Films* **1992**, *210/211*, 135-137.

(95)   Maget-Dana, R. The monolayer technique: a potent tool for studying the interfacial properties of antimicrobial and membrane-lytic peptides and their interactions with lipid membranes. *Biochim. Biophys. Acta* **1999**, *1462*, 109-140.

(96)   Deleu, M.; Paquot, M.; Nylander, T. Fengycin interaction with lipid monolayers at the air-aqueous interface--implications for the efect of fengycin on biological membranes. *J. Colloid Interface Sci.* **2005**, *283*, 358-365.

(97)   Viswanath, P.; Suresh, K. A. Polar head group interactions in mixed Langmuir monolayers. *Phys. Rev. E* **2003**, *67*, 061604-1-061604-8.

(98)   Więcek, A.; Dynarowicz-Łątka, P.; Miñones Jr., J.; Conde, O.; Casas, M. Interactions between an anticancer drug -edelfosine- and cholesterol in Langmuir monolayers. *Thin Solid Films* **2008**, *516*, 8829-8833.

(99)   Hao, C.; Sun, R.; Zhang, J.; Chang, Y.; Niu, C. Behavior of sulfatide/cholesterol mixed monolayers at the air/water interface. *Colloids Surf. B: Biont.* **2009**, *69*, 201-206.

(100)   Li, R.; Chen, Q.; Zhang, D.; Liu, H.; Hu, Y. Mixed monolayers of gemini surfactants and stearic acid at the air/water interface. *J. Colloid Interface Sci.* **2008**, *327*, 162-168.

(101)   Pack, D. W.; Arnold, F. H. Langmuir monolayer characterization of metal chelating lipids for protein targeting to membranes. *Chem. Phys. Lipids* **1997**, *86*, 135-152.

(102)   Weis, M.; Vančo, M.; Vitovič, P.; Hianik, T.; Cirák, J. Study of gramicidin A-phospholipid interactions in langmuir monolayers: analysis of their mechanical, thermodynamical, and electrical properties. *J. Phys. Chem. B* **2006**, *110*.

(103)   Eeman, M.; Pegado, L.; Dufrene, Y. F.; Paquot, M.; Deleu, M. Influence of environmental conditions on the interfacial organisation of fengycin, a bioactive lipopeptide produced by *Bacillus subtilis*. *J. Colloid Interface Sci.* **2009**, *329*, 253-264.

(104)   Goodrich, F. C. "Molecular interaction in mixed monolayers"; Proceeding of the Second International Congress of Surface Activity, 1957.